Distribution Category:
LMFBR—Components: Base
Technology (UC-79k)

ANL-82-71

ANL--82-71

DE83 004398

ARGONNE NATIONAL LABORATORY
9700 South Cass Avenue
Argonne, Illinois 60439

STABILITY OF TUBE ROWS IN CROSSFLOW

by

S. S. Chen and J. A. Jendrzejczyk

Components Technology Division

October 1982

TABLE OF CONTENTS

LIST OF ILLUSTRATIONS

LIST OF TABLES

NOMENCLATURE

NOMENCLATURE

D	Tube diameter
f	$\omega/2\pi$
f_i	Fluid force per unit length acting on tube i in the x direction
f_v	Reference frequency (= $\omega_v/2\pi$)
g_i	Fluid force per unit length acting on tube i in the y direction
ℓ	Tube length
ℓ_o	Tube length of overhung portion
m_i	Mass per unit length of tube i
m_v	Tube mass per unit length (= m_i)
P	Tube pitch
R	Tube radius
t	Time
T	Tube pitch in the direction 90° from that associated with the tube pitch P
U	Gap flow velocity
U_m	Mean gap flow velocity
u_i	Displacement of tube i in the x direction
U_v	Reduced flow velocity (= U_m/f_vD)
U_r	Reduced flow velocity (= U_m/fD, or U/f_vD)
U_e	Equivalent uniform flow velocity
v_i	Displacement of tube i in the y direction
x,y,z	Cartesian coordinates
$\alpha_{ij},\beta_{ij},\sigma_{ij},\tau_{ij}$	Fluid added-mass coefficients
$\dot{\alpha}_{ij},\dot{\beta}_{ij},\dot{\sigma}_{ij},\dot{\tau}_{ij}$	Hysteretic damping coefficients given in Eq. 3
$\bar{\alpha}'_{ij},\bar{\beta}'_{ij},\bar{\sigma}'_{ij},\bar{\tau}'_{ij}$	Viscous fluid-damping coefficients
$\alpha''_{ij},\beta''_{ij},\sigma''_{ij},\tau''_{ij}$	Fluidelastic-stiffness coefficients
$\alpha^d_{ij},\beta^d_{ij},\sigma^d_{ij},\tau^d_{ij}$	Effect
$\alpha^e_{ij},\beta^e_{ij},\sigma^e_{ij},\tau^e_{ij}$	Effect Eq. 1
γ_i	$\frac{\rho\pi R^2}{m_i}$
γ_v	Refere
δ_m	Mass-
ζ_1	Modal
τ	$\omega_v t$
ζ_i	Modal
ζ_v	Refer
η_i	Modal
ρ	Fluid
$\phi(z)$	Flow-v
$\psi(z)$	Modal
ω	Circul
ω_v	Refere
ω_i	Natura in vac
Ω_1	Natura
Ω_i	Natur

n

ed

NOMENCLATURE

$\alpha^d_{ij}, \beta^d_{ij}, \sigma^d_{ij}, \tau^d_{ij}$	Effective fluid-damping coefficient given in Eq. 14
$\alpha^e_{ij}, \beta^e_{ij}, \sigma^e_{ij}, \tau^e_{ij}$	Effective fluidelastic-stiffness coefficients given in Eq. 14
γ_i	$\frac{\rho\pi R^2}{m_i}$
γ_v	Reference mass ratio
δ_m	Mass-damping parameters ($= 2\pi\zeta_v m_v/\rho D^2$)
ζ_1	Modal damping ratio in flow
τ	$\omega_v t$
ζ_i	Modal damping ratio of tube i in the x direction
ζ_v	Reference modal damping ratio
η_i	Modal damping ratio of tube i in the y direction
ρ	Fluid density
$\phi(z)$	Flow-velocity distribution function
$\psi(z)$	Modal function of tube vibration
ω	Circular frequency of oscillation
ω_v	Reference circular frequency
ω_i	Natural frequency (rad/sec) of tube i in the x direction in vacuum
Ω_1	Natural frequency in flow
Ω_i	Natural frequency of tube i in the y direction in vacuum

STABILITY OF TUBE ROWS IN CROSSFLOW

by

S. S. Chen and J. A. Jendrzejczyk

ABSTRACT

A mathematical model for the instability of tube rows subjected to crossflow is examined. The theoretical model, based on the fluid-force data for a pitch-to-diameter ratio of 1.33, provides additional insight into the instability phenomenon. Tests are also conducted for three sets of tube rows. The effects of mass ratio, tube pitch, damping, detuning and finned tubes are investigated. Theoretical results and experimental data are in good agreement.

I. INTRODUCTION

High-velocity flow across a tube array can cause tube instability, which may result in extensive tube damage in a short time. Therefore, tube instability must be avoided in heat-exchanger tube bundles.

The prediction of instability flow velocity remains a difficult task. Various empirical correlations have been proposed to establish the instability flow velocity as a function of the mass-damping parameter.[1] These empirical correlations are used extensively in design. However, the detailed instability mechanisms of various tube arrangements are not well understood.

Based on a linear model and fluid forces measured for oscillating-tube arrays, Chen has established two basic instability mechanisms: fluid-damping-controlled instability and fluidelastic-stiffness-controlled instability.[2] For a tube row with a pitch-to-diameter ratio of 1.33, fluid-damping-controlled instability is dominant for a small mass-damping parameter and fluidelastic-stiffness-controlled instability is dominant for large mass-damping parameters. Experiments to verify the various features of instability for tube rows have been published.[3]

This report presents additional analytical results and experimental data of tube rows in crossflow. Analyses and tests are conducted for tube rows to investigate the effects of various system parameters. Specifically, this study includes the following investigations:

- The mathematical model is reexamined using a new definition of fluid-damping coefficients.
- The role of mass ratio and modal-damping ratio is examined for heavy fluid.
- Tube rows with a pitch-to-diameter ratio of 1.25 and 1.35 are tested.
- The effect of finned tubes on the critical flow velocity is studied.
- The inconsistency of various published experimental data at low mass-damping parameters is discussed.

The results of the study support the validity of the mathematical model and shed some additional light on the instability criteria.

II. THEORY

A. Fluid-Force Coefficients for Tube Arrays

Consider a group of n tubes vibrating in a flow as shown in Fig. 1. The axes of the tubes are parallel to one another and perpendicular to the x-y plane. Each tube has the same radius R, and the fluid is flowing with a gap flow velocity U. The displacement components of tube i in the x and y directions are u_i and v_i, respectively. The motion-dependent fluid-force components acting on tube i in the x and y directions are f_i and g_i, respectively; f_i and g_i are given as[2]

$$f_i = -\rho\pi R^2 \sum_{j=1}^{n} \left(\alpha_{ij} \frac{\partial^2 u_j}{\partial t^2} + \sigma_{ij} \frac{\partial^2 v_j}{\partial t^2}\right)$$

$$-\rho RU \sum_{j=1}^{n} \left(\bar{\alpha}'_{ij} \frac{\partial u_j}{\partial t} + \bar{\sigma}'_{ij} \frac{\partial v_j}{\partial t}\right)$$

$$+ \rho U^2 \sum_{j=1}^{n} \left(\alpha''_{ij} u_j + \sigma''_{ij} v_j\right) \qquad (1)$$

and

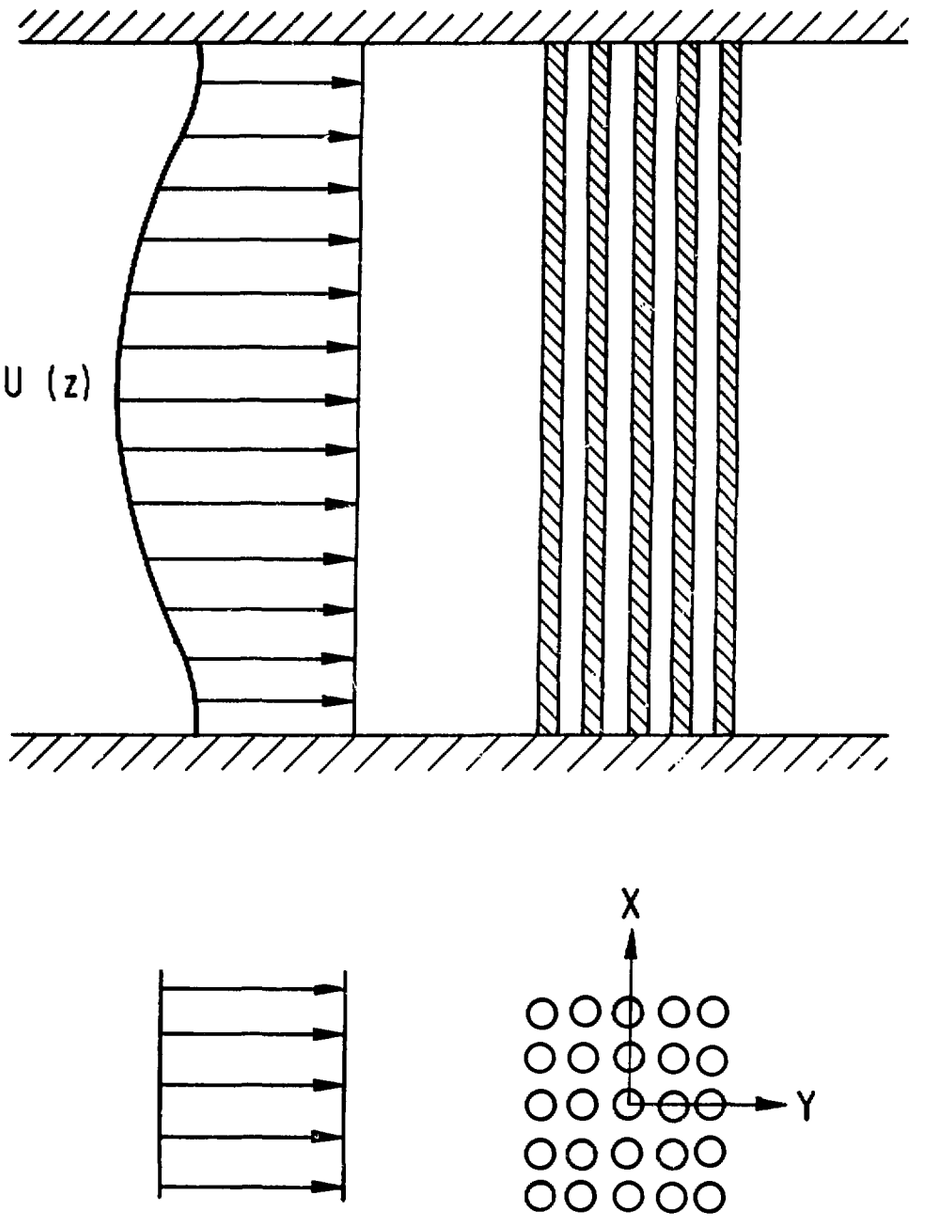

Fig. 1. An Array of Tubes in Crossflow

$$g_i = -\rho\pi R^2 \sum_{j=1}^{n} \left(\tau_{ij} \frac{\partial^2 u_j}{\partial t^2} + \beta_{ij} \frac{\partial^2 v_j}{\partial t^2}\right)$$

$$- \rho RU \sum_{j=1}^{n} \left(\bar{\tau}'_{ij} \frac{\partial u_j}{\partial t} + \bar{\beta}'_{ij} \frac{\partial v_j}{\partial t}\right)$$

$$+ \rho U^2 \sum_{j=1}^{n} \left(\tau''_{ij} u_j + \beta''_{ij} v_j\right). \tag{2}$$

Based on Eqs. 1 and 2, for large reduced flow velocity U_r (= $\pi U/R\omega$, where ω is the circular frequency of oscillation), the absolute values of the fluid-damping coefficients $\bar{\alpha}'_{ij}$, $\bar{\sigma}'_{ij}$, $\bar{\tau}'_{ij}$, and $\bar{\beta}'_{ij}$ increase linearly with reduced velocity.[2] Therefore, if these fluid-damping coefficients are divided by the reduced flow velocity, they will become constant at high reduced flow velocity. Let

$$\dot{\alpha}_{ij} = -\frac{R\omega}{U} \bar{\alpha}'_{ij},$$

$$\dot{\sigma}_{ij} = -\frac{R\omega}{U} \bar{\sigma}'_{ij},$$

$$\dot{\tau}_{ij} = -\frac{R\omega}{U} \bar{\tau}'_{ij}, \tag{3}$$

and

$$\dot{\beta}_{ij} = -\frac{R\omega}{U} \bar{\beta}'_{ij}.$$

Using Eqs. 1-3 yields

$$f_1 = -\rho\pi R^2 \sum_{j=1}^{n} \left(\alpha_{ij} \frac{\partial^2 u_j}{\partial t^2} + \sigma_{ij} \frac{\partial^2 v_j}{\partial t^2}\right)$$

$$+ \frac{\rho U^2}{\omega} \sum_{j=1}^{n} \left(\dot{\alpha}_{ij} \frac{\partial u_j}{\partial t} + \dot{\sigma}_{ij} \frac{\partial v_j}{\partial t}\right)$$

$$+ \rho U^2 \sum_{j=1}^{n} \left(\alpha''_{ij} u_j + \sigma''_{ij} v_j\right) \tag{4}$$

and

$$g_i = -\rho\pi R^2 \sum_{j=1}^{n} \left(\tau_{ij} \frac{\partial^2 u_j}{\partial t^2} + \beta_{ij} \frac{\partial^2 v_j}{\partial t^2}\right)$$

$$+ \frac{\rho U^2}{\omega} \sum_{j=1}^{n} \left(\dot{\tau}_{ij} \frac{\partial u_j}{\partial t} + \dot{\beta}_{ij} \frac{\partial v_j}{\partial t}\right)$$

$$+ \rho U^2 \sum_{j=1}^{n} \left(\tau''_{ij} u_j + \beta''_{ij} v_j\right). \tag{5}$$

Fluid forces acting on tube arrays were measured and reported recently by Tanaka and his colleague for a row of tubes and square arrays.[4-6] In their tests, fluid-force components are measured as functions of tube displacements. For example, tube j is excited in the y direction; its displacement in the y direction is given by

$$v_j = v \exp(\sqrt{-1}\ \omega t), \tag{6}$$

where ω is the oscillation frequency of cylinder j. The fluid force acting on tube i in the x direction is given by

$$f_i = \frac{1}{2}\ \rho U^2 (c_{ij}\cos\phi_{ij} + \sqrt{-1}\ c_{ij}\sin\phi_{ij})v, \tag{7}$$

where c_{ij} is the fluid-force amplitude and ϕ_{ij} is the phase angle between the fluid force and the tube displacement. These values are obtained by Tanaka for three tube arrays.

Using Eqs. 4 and 5, we can also write the fluid force component as

$$f_i = (\rho\pi R^2 \omega^2 \sigma_{ij} + \rho U^2 \sigma''_{ij} + \sqrt{-1}\ \rho U^2 \dot{\sigma}_{ij})v. \tag{8}$$

Comparing Eqs. 7 and 8 yields

$$\sigma''_{ij} - \frac{1}{2}\ c_{ij}\cos\phi_{ij} - \frac{\pi^3}{U_r^2}\ \sigma_{ij} \tag{9}$$

and

$$\dot{\sigma}_{ij} = \frac{1}{2}\ c_{ij}\sin\phi_{ij},$$

where U_r is the reduced flow velocity ($U_r = \pi U/\omega R$).

Figures 2-5 show values of $\dot{\alpha}_{ij}$, $\dot{\sigma}_{ij}$, $\dot{\tau}_{ij}$, $\dot{\beta}_{ij}$ and α''_{ij}, σ''_{ij}, τ''_{ij}, and β''_{ij} for a tube row and two square arrays reduced from Tanaka's data.

Note that fluid damping is modeled as viscous damping in Eqs. 1 and 2 with damping coefficients $\bar{\alpha}'_{ij}$, $\bar{\sigma}'_{ij}$, $\bar{\tau}'_{ij}$, and $\bar{\beta}'_{ij}$, and hysteretic damping in Eqs. 4 and 5 with damping coefficients $\dot{\alpha}_{ij}$, $\dot{\sigma}_{ij}$, $\dot{\tau}_{ij}$, and $\dot{\beta}_{ij}$. For small U_r, the hysteretic damping coefficients are functions of U_r. For large U_r, these coefficients are practically constant and are more convenient to use.

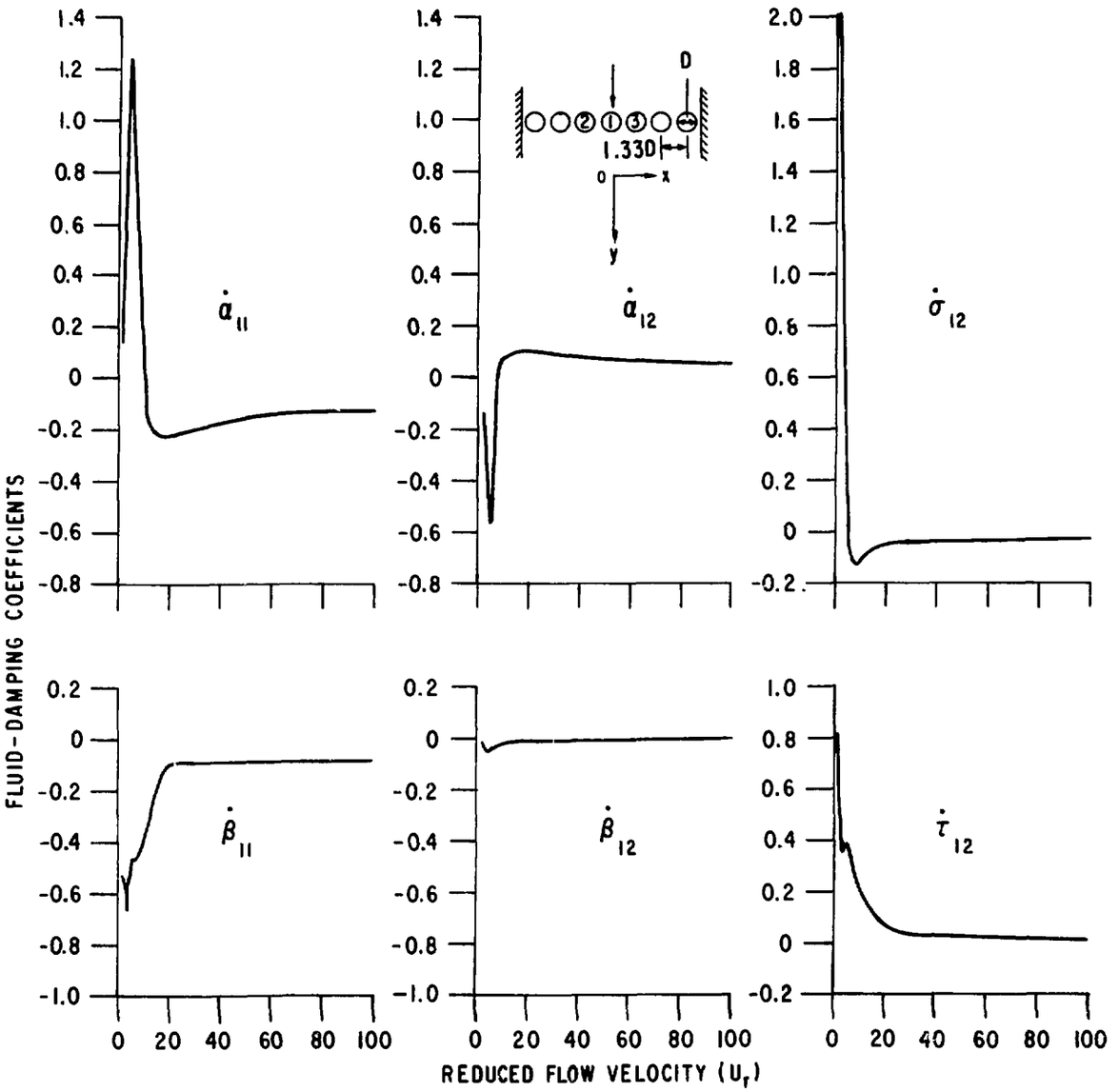

Fig. 2. Fluid-damping Coefficients for a Row of Tubes

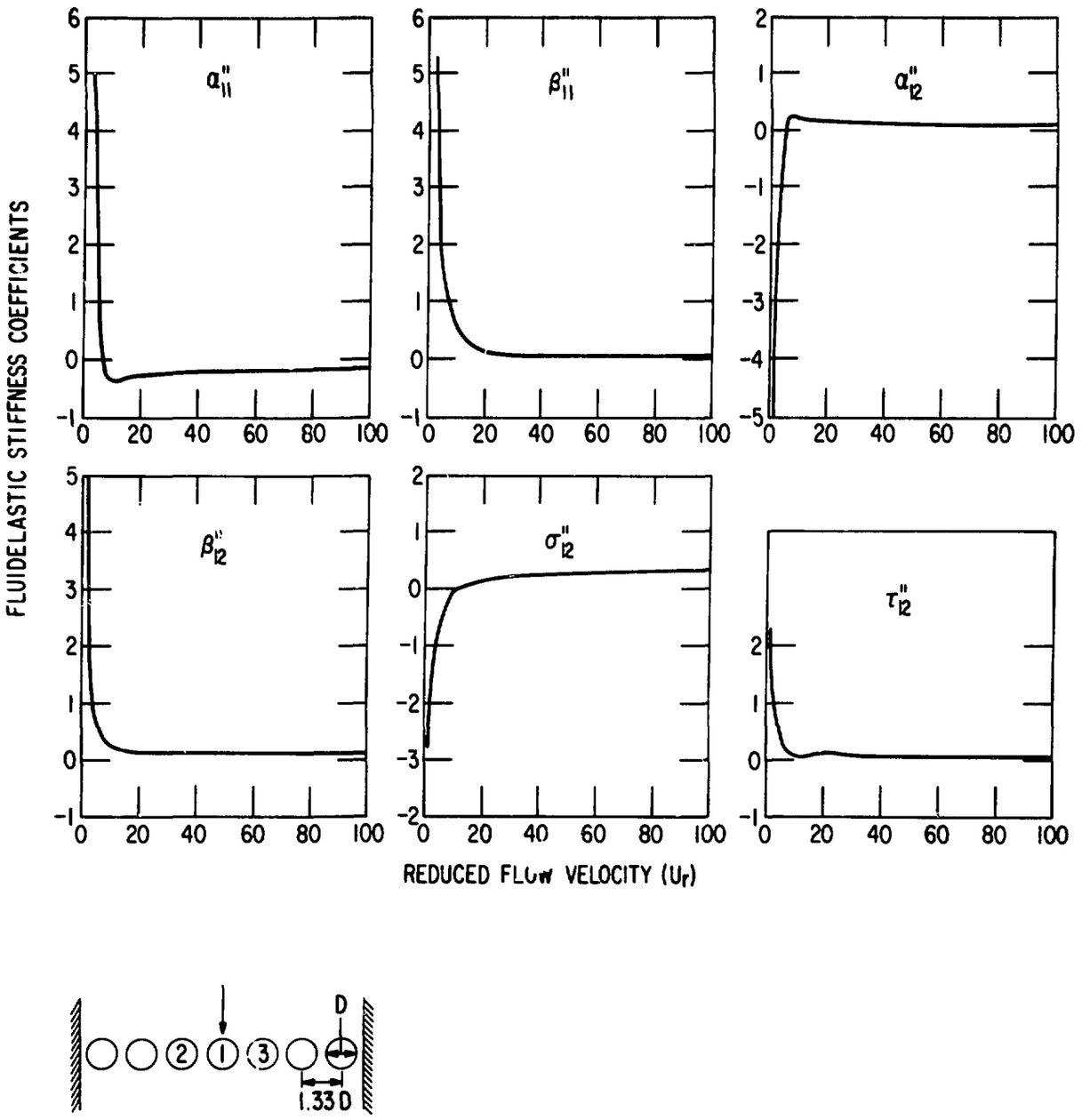

Fig. 3. Fluidelastic-stiffness Coefficients for a Row of Tubes

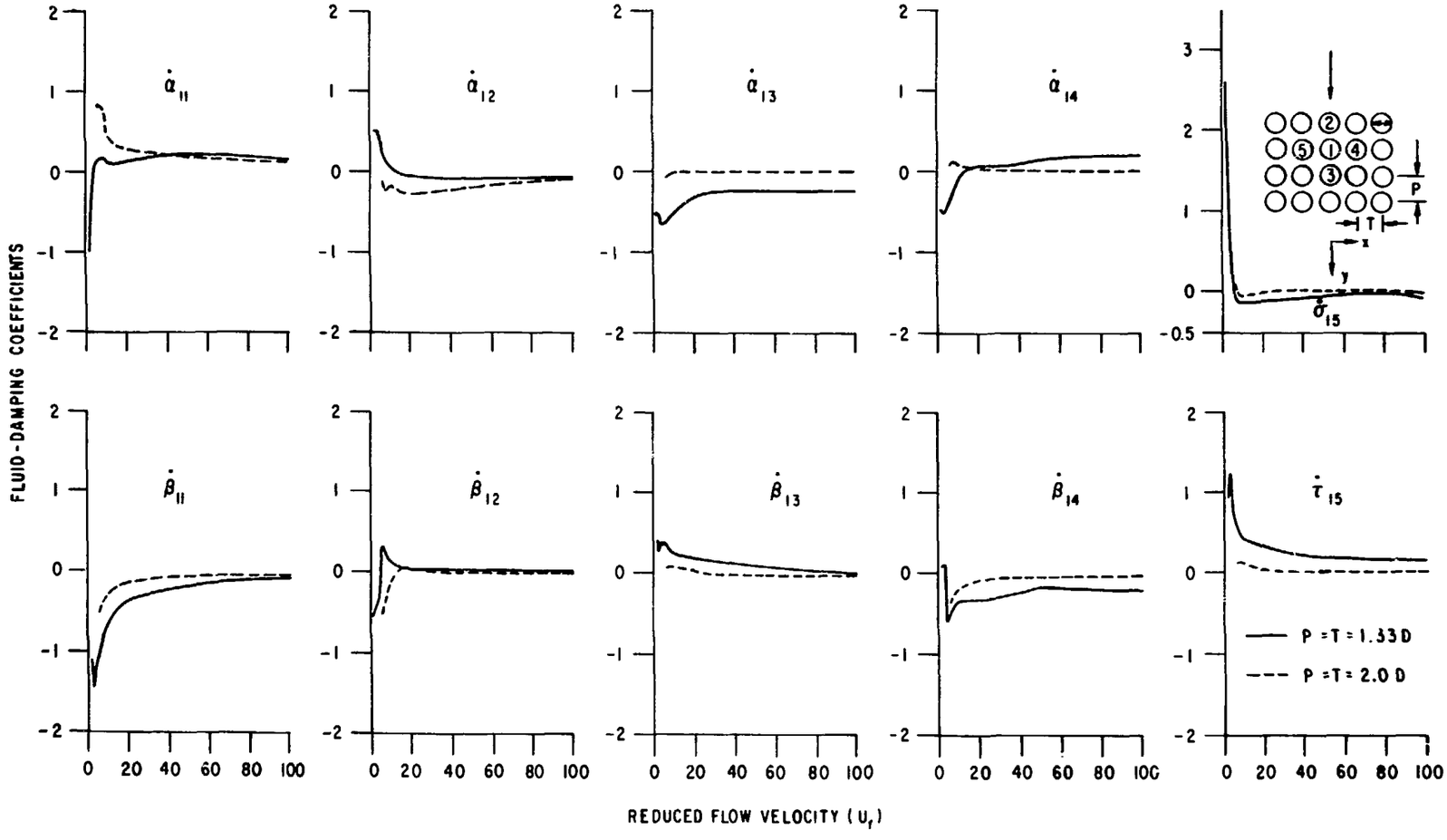

Fig. 4. Fluid-damping Coefficients for Square Tube Arrays

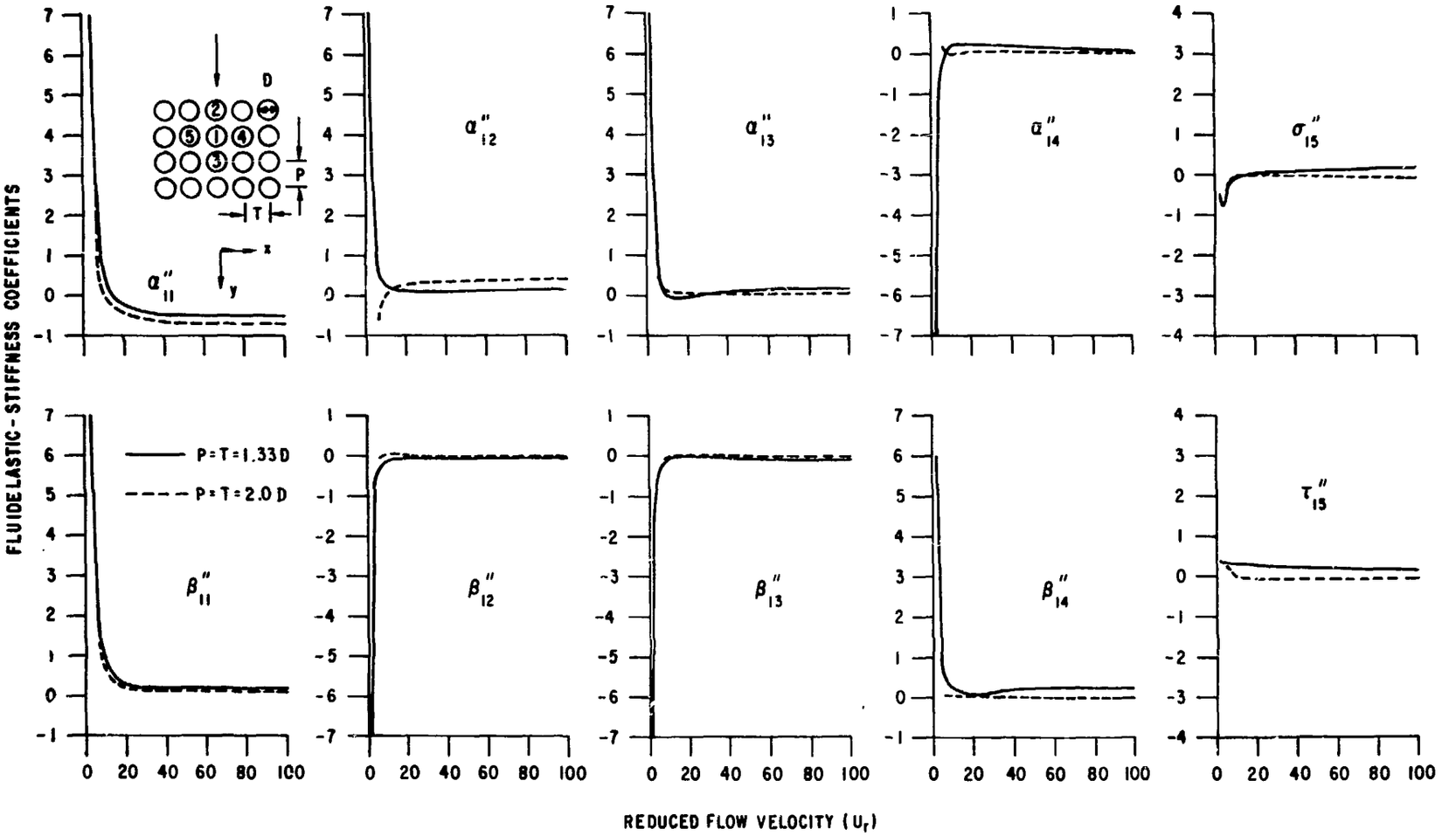

Fig. 5. Fluidelastic-stiffness Coefficients for Square Tube Arrays

B. Analysis

The in-vacuum variables associated with the tube motion in the x direction are displacement u_i, mass per unit length m_i, modal damping ζ_i, and natural frequency ω_i. The corresponding variables in the y direction are v_i, m_i, η_i, and Ω_i. The modal function of the tube vibrating in vacuum and in fluid is $\psi(z)$;

$$\frac{1}{\ell}\int_0^{\ell}\psi^2(z)dz = 1, \tag{10}$$

where ℓ is the length of the tubes. Let

$$u_i(z,t) = a_i(t)\psi(z)$$

and (11)

$$v_i(z,t) = b_i(t)\psi(z),$$

where $a_i(t)$ and $b_i(t)$ are functions of time only. Assume that the flow-velocity distribution is given by

$$U(z) = U_m\phi(z). \tag{12}$$

The equations of motion for tube rows are[2]

$$\begin{aligned}
&\frac{d^2a_i}{dt^2} + 2\zeta_i\omega_i\frac{da_i}{dt} + \omega_i^2a_i + \frac{\rho\pi R^2}{m_i}\sum_{j=1}^{n}\left(\alpha_{ij}\frac{d^2a_j}{dt^2} + \sigma_{ij}\frac{d^2b_j}{dt^2}\right)\\
&\quad - \frac{\rho U_m^2}{m_i\omega}\sum_{j=1}^{n}\left(\alpha_{ij}^d\frac{da_j}{dt} + \sigma_{ij}^d\frac{db_j}{dt}\right)\\
&\quad - \frac{\rho U_m^2}{m_i}\sum_{j=1}^{n}\left(\alpha_{ij}^e a_j + \sigma_{ij}^e b_j\right) = 0
\end{aligned}$$

and (13)

$$\begin{aligned}
&\frac{d^2b_j}{dt^2} + 2\eta_i\Omega_i\frac{db_j}{dt} + \Omega_i^2b_i + \frac{\rho\pi R^2}{m_i}\sum_{j=1}^{n}\left(\tau_{ij}\frac{d^2a_j}{dt^2} + \beta_{ij}\frac{d^2b_j}{dt^2}\right)\\
&\quad - \frac{\rho U_m^2}{m_i\omega}\sum_{j=1}^{n}\left(\tau_{ij}^d\frac{da_j}{dt} + \beta_{ij}^d\frac{db_j}{dt}\right)\\
&\quad - \frac{\rho U_m^2}{m_i}\sum_{j=1}^{n}\left(\tau_{ij}^e a_j + \beta_{ij}^e b_j\right) = 0,
\end{aligned}$$

where

$$\alpha_{ij}^{d} = \frac{1}{\ell}\int_0^{\ell} \dot{\alpha}_{ij}\phi^2\psi^2 dz, \qquad \alpha_{ij}^{e} = \frac{1}{\ell}\int_0^{\ell} \ddot{\alpha}_{ij}\phi^2\psi^2 dz,$$

$$\sigma_{ij}^{d} = \frac{1}{\ell}\int_0^{\ell} \dot{\sigma}_{ij}\phi^2\psi^2 dz, \qquad \sigma_{ij}^{e} = \frac{1}{\ell}\int_0^{\ell} \ddot{\sigma}_{ij}\phi^2\psi^2 dz,$$

$$\tau_{ij}^{d} = \frac{1}{\ell}\int_0^{\ell} \dot{\tau}_{ij}\phi^2\psi^2 dz, \qquad \tau_{ij}^{e} = \frac{1}{\ell}\int_0^{\ell} \ddot{\tau}_{ij}\phi^2\psi^2 dz, \tag{14}$$

$$\beta_{ij}^{d} = \frac{1}{\ell}\int_0^{\ell} \dot{\beta}_{ij}\phi^2\psi^2 dz, \qquad \beta_{ij}^{e} = \frac{1}{\ell}\int_0^{\ell} \ddot{\beta}_{ij}\phi^2\psi^2 dz.$$

Hysteretic fluid damping is used in Eq. 13.

Let ω_v be the reference circular frequency, which may be the natural frequency of a particular tube in vacuum. Using the dimensionless parameters

$$\tau = \omega_v t,$$

$$U_v = \frac{U_m}{f_v D} \qquad \left(f_v = \frac{\omega_v}{2\pi}\right), \tag{15}$$

and

$$\gamma_i = \frac{\rho\pi R^2}{m_i},$$

Eqs. 13 become

$$\ddot{a}_i + \gamma_i \sum_{j=1}^{n} \left(\alpha_{ij}\ddot{a}_j + \sigma_{ij}\ddot{b}_j\right)$$

$$+ 2\zeta_i\left(\frac{\omega_i}{\omega_v}\right)\dot{a}_i - \frac{\gamma_i}{\pi}U_v^2 \sum_{j=1}^{n}\left(\alpha_{ij}^{d}\dot{a}_j + \sigma_{ij}^{d}\dot{b}_j\right)$$

$$+ \left(\frac{\omega_i}{\omega_v}\right)^2 a_i - \frac{\gamma_i}{\pi^3}U_v^2 \sum_{j=1}^{n}\left(\alpha_{ij}^{e}a_j + \sigma_{ij}^{e}b_j\right) = 0 \tag{16}$$

and

$$\ddot{b}_i + \gamma_i \sum_{j=1}^{n} (\tau_{ij}\ddot{a}_j + \beta_{ij}\ddot{b}_j)$$

$$+ 2\eta \left(\frac{\Omega_i}{\omega_v}\right) \dot{b}_i - \frac{\gamma_i}{\pi^3} U_v^2 \sum_{j=1}^{n} (\tau_{ij}^d \dot{a}_j + \beta_{ij}^d \dot{b}_j)$$

$$+ \left(\frac{\Omega_i}{\omega_v}\right)^2 b_i - \frac{\gamma_i}{\pi^3} U^2 \sum_{j=1}^{n} (\tau_{ij}^e a_j + \beta_{ij}^e b_j) = 0, \qquad (16)$$

(Contd.)

where the dot denotes differentiation with respect to τ. Fluid-damping coefficients and fluidelastic-stiffness coefficients are functions of reduced flow velocity U_r ($= U_m/fD$). The frequency of oscillation f ($= \omega/2\pi$) is different from the reference frequency f_v.

The stability of a tube array is determined from Eqs. 16. The non-dimensional parameters in Eqs. 16 are γ_i, ω_i/ω_v, Ω_i/ω_v, ζ_i, η_i, U_v, α_{ij}, σ_{ij}, τ_{ij}, β_{ij}, α_{ij}^d, σ_{ij}^d, τ_{ij}^d, β_{ij}^d, α_{ij}^e, σ_{ij}^e, τ_{ij}^e, and β_{ij}^e. Therefore, the critical flow velocity can be written in a functional form:

$$U_v = F(\gamma_i, \omega_i/\omega_v, \Omega_i/\omega_v, \zeta_i, \eta_i, \alpha_{ij}, \sigma_{ij}, \tau_{ij}, \beta_{ij},$$
$$\alpha_{ij}^d, \sigma_{ij}^d, \tau_{ij}^d, \beta_{ij}^d, \alpha_{ij}^e, \sigma_{ij}^e, \tau_{ij}^e, \beta_{ij}^e) . \qquad (17)$$

These parameters can be divided into several groups.

(a) Mass Ratio (γ_i): This represents the displaced mass of fluid to the tube mass. In most practical applications, all tubes are identical; therefore,

$$\gamma_i = \gamma_v , \quad i = 1, 2, 3, \ldots, n. \qquad (18)$$

(b) Detuning in Frequency (ω_i/ω_v and Ω_i/ω_v): Frequency variations of different tubes in a tube array and of the same tube in the two directions can affect stability. For an in-tune tube array,

$$\omega_i = \Omega_i = \omega_v, \quad i = 1, 2, 3, \ldots, n. \qquad (19)$$

(c) Detuning in Damping (ζ_i and η_i): Detuning in damping can also affect stability. For a tube array without damping variation,

$$\zeta_i = \eta_i = \zeta_v, \quad i = 1, 2, 3, \ldots, n. \qquad (20)$$

(d) Added Mass Coefficients (α_{ij}, σ_{ij}, τ_{ij}, and β_{ij}): These coefficients depend on tube arrangement only. For a given tube array, they are constants.

(e) Effective Fluid-damping Coefficients (α^d_{ij}, σ^d_{ij}, τ^d_{ij}, and β^d_{ij}): These coefficients depend on flow-velocity distribution function $\phi(z)$, tube mode shape $\psi(z)$, and fluid-damping coefficients $\dot{\alpha}_{ij}$, $\dot{\sigma}_{ij}$, $\dot{\tau}_{ij}$, and $\dot{\beta}_{ij}$. Fluid-damping coefficients are a function of the reduced flow velocity U_r for small U_r and approximately constants for large U_r.

(f) Effective Fluidelastic-stiffness Coefficients (α^e_{ij}, σ^e_{ij}, τ^e_{ij}, and β^e_{ij}): These coefficients are functions of flow-velocity distribution function $\phi(z)$, tube mode shape $\psi(z)$, and fluidelastic-stiffness coefficients α''_{ij}, σ''_{ij}, τ''_{ij}, and β''_{ij}. In general, fluidelastic-stiffness coefficients are functions of the reduced flow velocity U_r; however, for large U_r, they are very weak functions of U_r and can be considered as constants.

For a tube array, in which all tubes are identical, having the same natural frequency and damping in both directions, using Eqs. 16, and 18-20 yields

$$\ddot{a}_i + \gamma_v \sum_{j=1}^{n} (\alpha \ddot{a} + \sigma_{ij} \ddot{b}_j) + 2\zeta_v \dot{a}_i - \frac{\gamma_v}{\pi^3} U_v^2 \sum_{j=1}^{n} (\alpha^d_{ij} \dot{a}_j + \sigma^d_{ij} \dot{b}_j) + a_i - \frac{\gamma_v}{\pi^3} U_v^2 \sum_{j=1}^{n} (\alpha^e_{ij} a_j + \sigma^e_{ij} b_j) = 0 \qquad (21)$$

and

$$\ddot{b}_i + \gamma_v \sum_{j=1}^{n} (\tau_{ij} \ddot{a}_j + \beta_{ij} \ddot{b}_j) + 2\zeta_v \dot{b}_i - \frac{\gamma_v}{\pi^3} U_v^2 \sum_{j=1}^{n} (\tau^d_{ij} \dot{a}_j + \beta^d_{ij} \dot{b}_j) + b_i - \frac{\gamma_v}{\pi^3} U_v^2 \sum_{j=1}^{n} (\tau^e_{ij} a_j + \beta^e_{ij} b_j) = 0, \qquad (22)$$

and using Eqs. 17-20 yields

$$U_v = F(\gamma_v, \zeta_v, \alpha_{ij}, \sigma_{ij}, \tau_{ij}, \beta_{ij}, \alpha^d_{ij}, \sigma^d_{ij}, \tau^d_{ij}, \beta^d_{ij}, \alpha^e_{ij}, \sigma^e_{ij}, \tau^e_{ij}, \beta^e_{ij}). \tag{23}$$

The dynamic characteristics can be studied based on Eqs. 13 or 16. Approximate solutions based on constrained mode provide significant insight into the system characteristics.

Consider tube 1 oscillating in the x direction. The equation of motion is

$$\ddot{a}_1 + 2\zeta_1 \Omega_1 \dot{a}_1 + \Omega_1^2 a_1 = 0, \tag{24}$$

where

$$\Omega_1 = \omega_v \left(\frac{1 - \frac{1}{\pi^3} \gamma_v U_v^2 \alpha^e_{11}}{1 + \alpha_{11} \gamma_v} \right)^{1/2}$$

and (25)

$$\zeta_1 = \frac{\zeta_v - \frac{1}{2\pi^3} \gamma_v U_v^2 \alpha^d_{11}}{[(1 + \gamma_v \alpha_{11})(1 - \frac{1}{\pi^3} \gamma_v U_v^2 \alpha^e_{11})]^{1/2}},$$

where Ω_1 and ζ_1 are the circular natural frequency and modal damping ratio of the constrained mo' in flow. The critical flow velocity can be determined from Eq. 25:

$$\zeta_1 = 0; \quad \text{i.e., } U_v = \left(\frac{2\pi^3 \zeta_v}{\gamma_v \alpha^d_{11}} \right)^{1/2} \tag{26}$$

$$\text{or } \frac{U_m}{f_v D} = \left(\frac{4\pi}{\alpha^d_{11}} \right)^{0.5} \left(\frac{2\pi \zeta_v m_v}{\rho D^2} \right)^{0.5}. \tag{27}$$

Similarly, oscillations in the y direction can be analyzed; the results are similar to those given in Eqs. 24-27.

For constrained modes involving multiple tubes oscillating in a particular pattern, similar results are obtained. For example, consider the case in which all tubes are moving in the x direction with the same amplitude. The equation of motion becomes

$$\ddot{a}_1 + 2\zeta_1 \Omega_1 \dot{a}_1 + \Omega_1^2 a_1 = 0, \tag{28}$$

where

$$\Omega_1 = \omega_v \left(\frac{1 - \frac{1}{\pi^3} \gamma_v U_v^2 \alpha_1^e}{1 + \alpha_1 \gamma_v} \right)^{1/2},$$

$$\zeta_1 = \frac{\zeta_v - \frac{1}{2\pi^3} \gamma_v U_v^2 \alpha_1^d}{\left[(1 + \gamma_v \alpha_1)\left(1 - \frac{1}{\pi^3} \gamma_v U_v^2 \alpha_1^e\right) \right]^{1/2}}, \tag{29}$$

$$\alpha_1^e = \frac{1}{\ell} \int_0^\ell \left(\sum_{j=1}^n \alpha_{1j} \right) \phi^2 \psi^2 dz,$$

and

$$\alpha_1^d = \frac{1}{\ell} \int_0^\ell \left(\sum_{j=1}^n \dot{\alpha}_{1j} \right) \phi^2 \psi^2 dz.$$

The critical flow velocity is given by

$$\frac{U_m}{f_v D} = \left(\frac{4\pi}{\alpha_1^d} \right)^{0.5} \left(\frac{2\pi \zeta_v m_v}{\rho D^2} \right)^{0.5}. \tag{30}$$

For light fluids, the fluid inertia can be neglected; Eqs. 22 may be written

$$\ddot{a}_i + 2\zeta_v \dot{a}_i + a_i$$

$$- \frac{\gamma_v}{\pi^3} U_v^2 \sum_{j=1}^n \left(\alpha_{ij}^d \dot{a}_j + \sigma_{ij}^d \dot{b}_j + \alpha_{ij}^e a_j + \sigma_{ij}^e b_j \right) = 0$$

and (31)

$$\ddot{b}_i + 2\zeta_v \dot{b}_i + b_i$$

$$- \frac{\gamma_v}{\pi^3} U_v^2 \sum_{j=1}^{n} (\tau_{ij}^d \dot{a}_j + \beta_{ij}^d \dot{b}_j + \tau_{ij}^e a_j + \beta_{ij}^e b_j) = 0. \qquad (31)$$

(Contd.)

In light fluids, instability occurs at large U_v, and the fluid-force coefficients α_{ij}^d, σ_{ij}^d, τ_{ij}^d, β_{ij}^d, α_{ij}^e, σ_{ij}^e, τ_{ij}^e, and β_{ij}^e are approximately independent of U_v ($U_v \approx U_r$). In Eqs. 31, the variables controlling the system stability are the parameters ζ_v and $\gamma_v U_v^2$. Note that the role of $\gamma_v U_v^2$ is the same as ζ_v. The terms associated with ζ_v and $\gamma_v U_v^2$ in Eqs. 31 are contributing to system damping; the modal damping of a mode can be written as

$$\xi_1 = \zeta_v - C\gamma_v U_v^2, \qquad (32)$$

where C depends on the fluid-force coefficients. The instability will occur if $\xi_1 = 0$; i.e.,

$$U_v = \frac{1}{C} \left(\frac{\zeta_v}{\gamma_v}\right)^{0.5}, \qquad (33)$$

or

$$\frac{U_m}{f_v D} \propto \left(\frac{2\pi\zeta_v m_v}{\rho D^2}\right)^{0.5}. \qquad (34)$$

Thus for light fluid, the critical reduced flow velocity will be proportional to the half-power of the mass-damping parameter. This is true in both fluid-damping-controlled or fluidelastic-controlled instability as long as the critical reduced flow velocity is relatively large. At low reduced flow velocity U_v, since both fluid-damping and fluidelastic-stiffness coefficients are functions of U_r, no such conclusions can be made.

When a tube array is subjected to nonuniform flow, effective fluid-force coefficients must be calculated based on Eq. 14. At high U_r, the fluid-force coefficients are independent of U_r. An equivalent flow velocity can be defined as

$$U_e = U_m \left(\frac{1}{\ell} \int_0^{\ell} \phi^2 \psi^2 dz\right)^{1/2}. \qquad (35)$$

Equation 35 has been used by various investigators.[7-9]

At low reduced flow velocity, it is very difficult, if not impossible, to define an equivalent flow velocity. The critical flow velocity depends on the various integrals given in Eq. 14. Since all the fluid-damping and fluidelastic-stiffness coefficients are functions of the reduced flow velocity, it is unlikely an equivalent flow velocity can be found such that all integrals will be the same as the values based on the nonuniform flow distribution. For a constrained mode, neglecting the effect of the fluidelastic-stiffness force, an equivalent flow velocity U_e may be defined as

$$U_e^2 \alpha_{ij}^d = \frac{U_m^2}{\ell} \int_0^\ell \dot{\alpha}_{ij} \phi^2 \psi^2 dz. \tag{36}$$

Note that $\dot{\alpha}_{ij}$ depends on U_r, which in turn depends on z. At a given flow rate U_m, the integral in Eq. 36 can be calculated. The equivalent flow velocity is then given by

$$U_e = U_m \left(\frac{1}{\ell} \int_0^\ell \dot{\alpha}_{ij} \phi^2 \psi^2 dz / \alpha_{ij}^d \right)^{1/2}, \tag{37}$$

where α_{ij}^d is evaluated at the flow velocity U_e. Thus, it will require an iterative process to find an equivalent flow velocity.

C. Numerical Results

For this presentation, calculations for a standard case of a tube row with a pitch-to-diameter ratio of 1.33 are based on the following conditions: $\zeta_v = 2\%$, $\phi(z) = 1$, and all tubes being in tune.

Figure 6 shows the critical flow velocity as a function of the number of tubes in a row for several values of δ_m. For a tube array in which all tubes are in tune, the critical flow velocity decreases with the number of tubes; the decrease is more drastic for a small number of tubes. Also, the effect of the number of tubes on the fluidelastic-stiffness-controlled instability (δ_m = 20, 40, and 60) is more significant than on the fluid-damping instability (δ_m = 1). This effect can be explained qualitatively using the equations of motion and fluid-force coefficients. For small δ_m, tube instability is basically controlled by the coefficient $\dot{\alpha}_{ij}$, while at large δ_m it is controlled by τ_{ij}'' and σ_{ij}''. At low δ_m, instability can occur in an elastic tube surrounded by rigid tubes. But at large δ_m, at least two tubes are needed to cause instability.

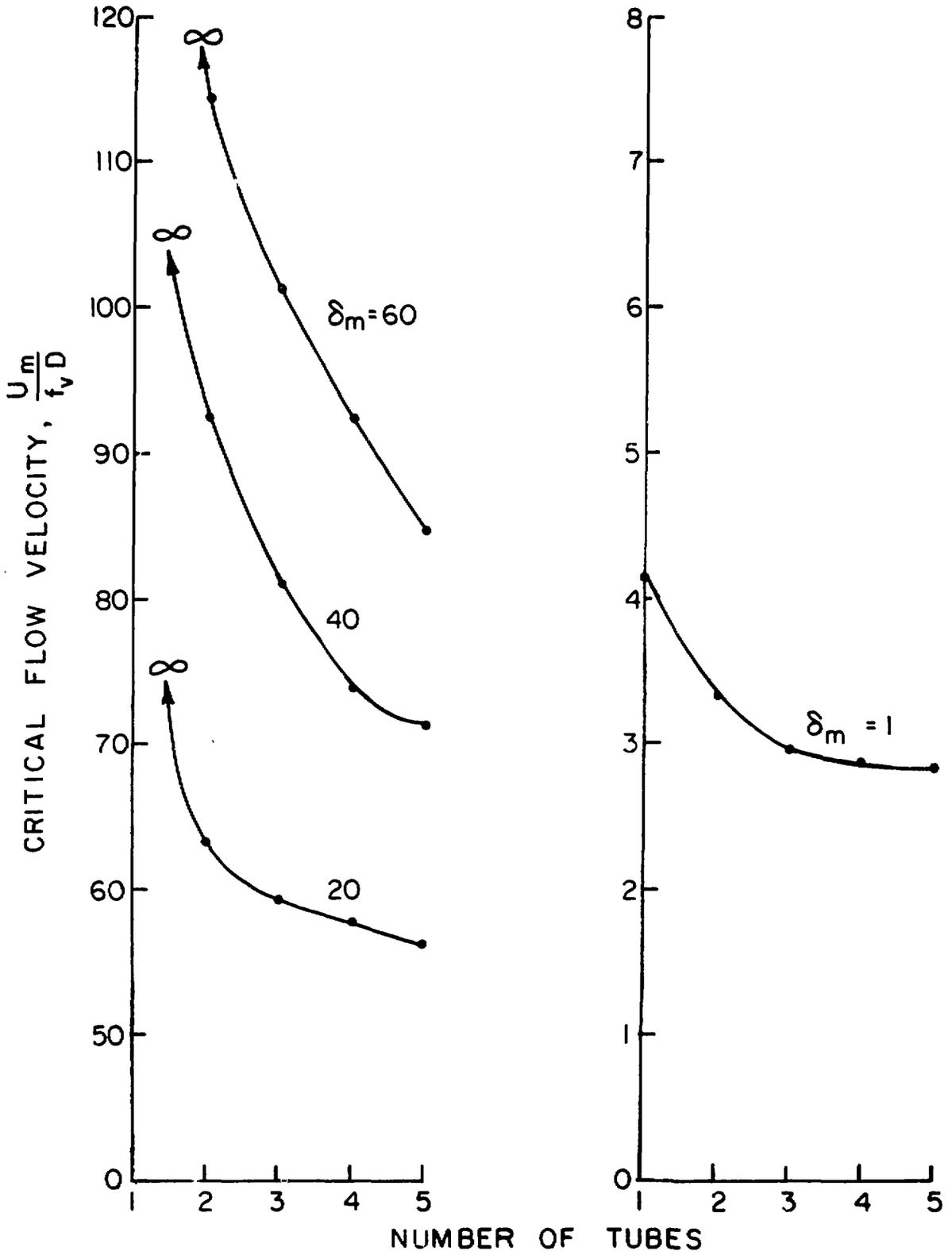

Fig. 6. The Critical Flow Velocity as a Function of the Number of Tubes

In different experiments conducted by different investigators, the number of tubes used is not the same. Therefore, even if all other parameters are the same, the instability flow velocity will be different.

Figures 7 and 8 show the stability map for a row of five and three tubes. For large δ_m, the results calculated for different set of ζ_v and $m_v/\rho D^2$ are about the same; i.e., the instability is independent of the individual values of ζ_v and $m_v/\rho D^2$, but dependent on the product of ζ_v and $m_v/\rho D^2$. At low δ_m, the results for different sets of ζ_v and $m_v/\rho D^2$ are not the same. In Fig. 7, the critical flow velocities are determined for a fixed ζ_v with variable $m_v/\rho D^2$ at low δ_m. It is seen that for a fixed δ_m, the critical flow velocity increases with decreasing ζ_v. In Fig. 8, the mass ratio is kept constant while ζ_v is variable. For a fixed δ_m, the critical flow velocity increases with decreasing mass ratio.

In the past, the two parameters ζ_v and $m_v/\rho D^2$ are frequently combined as a single parameter. This is applicable for large δ_m. For small δ_m, the two parameters have to be treated as two variables. Most of the experimental data reported are presented as a function of δ_m. Since different experiments are carried out for different sets of ζ_v and $m_v/\rho D^2$, even for the same δ_m, the critical flow velocity will be different. This is one of the reasons that there is more scattering in the data at low values of δ_m.

At δ_m equal to about 3 to 5, there is a finite jump in the critical flow velocity. The jump is attributed to the transition from fluid-damping-controlled instability to fluidelastic-stiffness-controlled instability. The values of δ_m at which the jump occurs depends on the values of damping ζ_v and γ_v. For smaller ζ_v in Fig. 7 and smaller γ_v in Fig. 8, the jump occurs at higher δ_m, and vice versa.

Figure 9 shows the instability modes for two, three, four, and five tubes in a row and for two values of δ_m. For $\delta_m = 1$, the instability is fluid-damping-controlled type. The motion is predominantly in the lift direction, and the tubes are moving out of phase. For $\delta_m = 40$, the instability is fluidelastic-stiffness-controlled type. The motion is a typically orbital path with some tubes moving predominantly in the drag direction and some tubes in the lift direction.

Figure 10 shows the ratio of critical flow velocities of a tube row consisting of detuned-tubes to a tube row consisting of in-tune tubes. In the detuned tube row, tube natural frequencies in the two directions are the same, and tubes 2 and 4 have higher natural frequency ω_B. In the in-tune tube row, all natural frequencies are ω_A. In this case, detuning tends to stabilize the system; i.e., the critical flow velocity increases with the increase in the frequency ratio ω_B/ω_A. Figure 10 shows that for $\delta_m = 20$, the critical flow increases significantly with ω_B/ω_A. However,

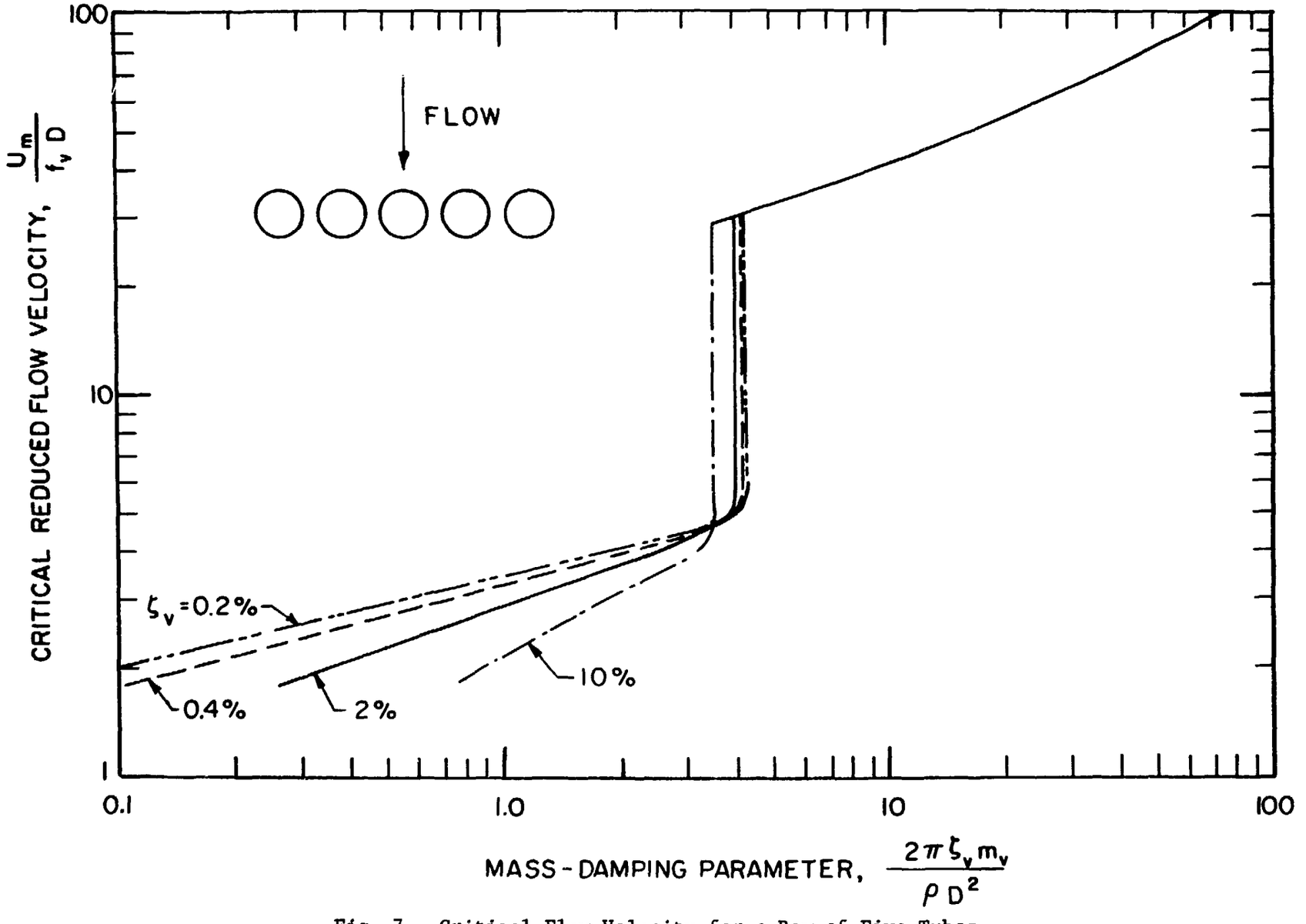

Fig. 7. Critical Flow Velocity for a Row of Five Tubes

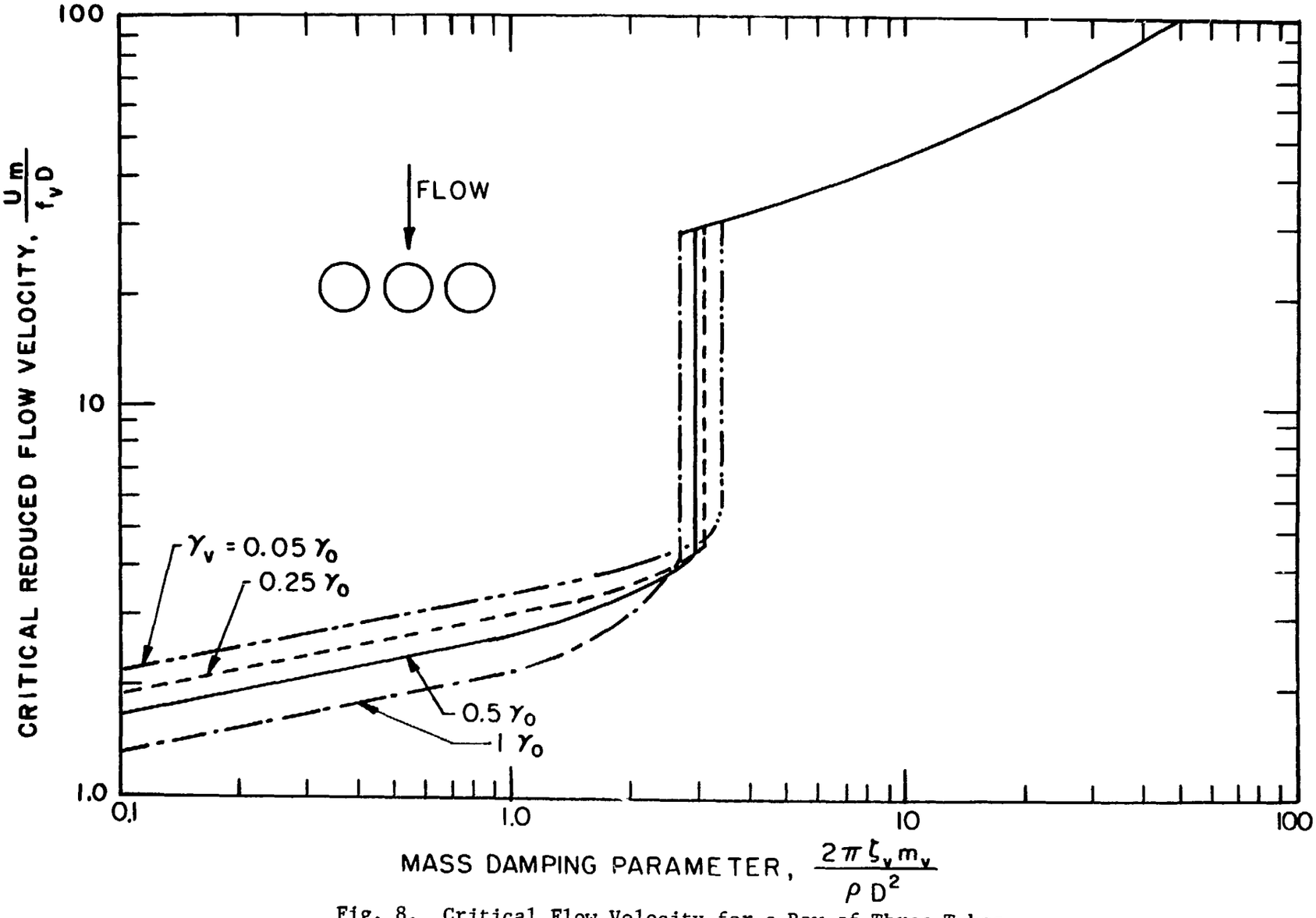

Fig. 8. Critical Flow Velocity for a Row of Three Tubes

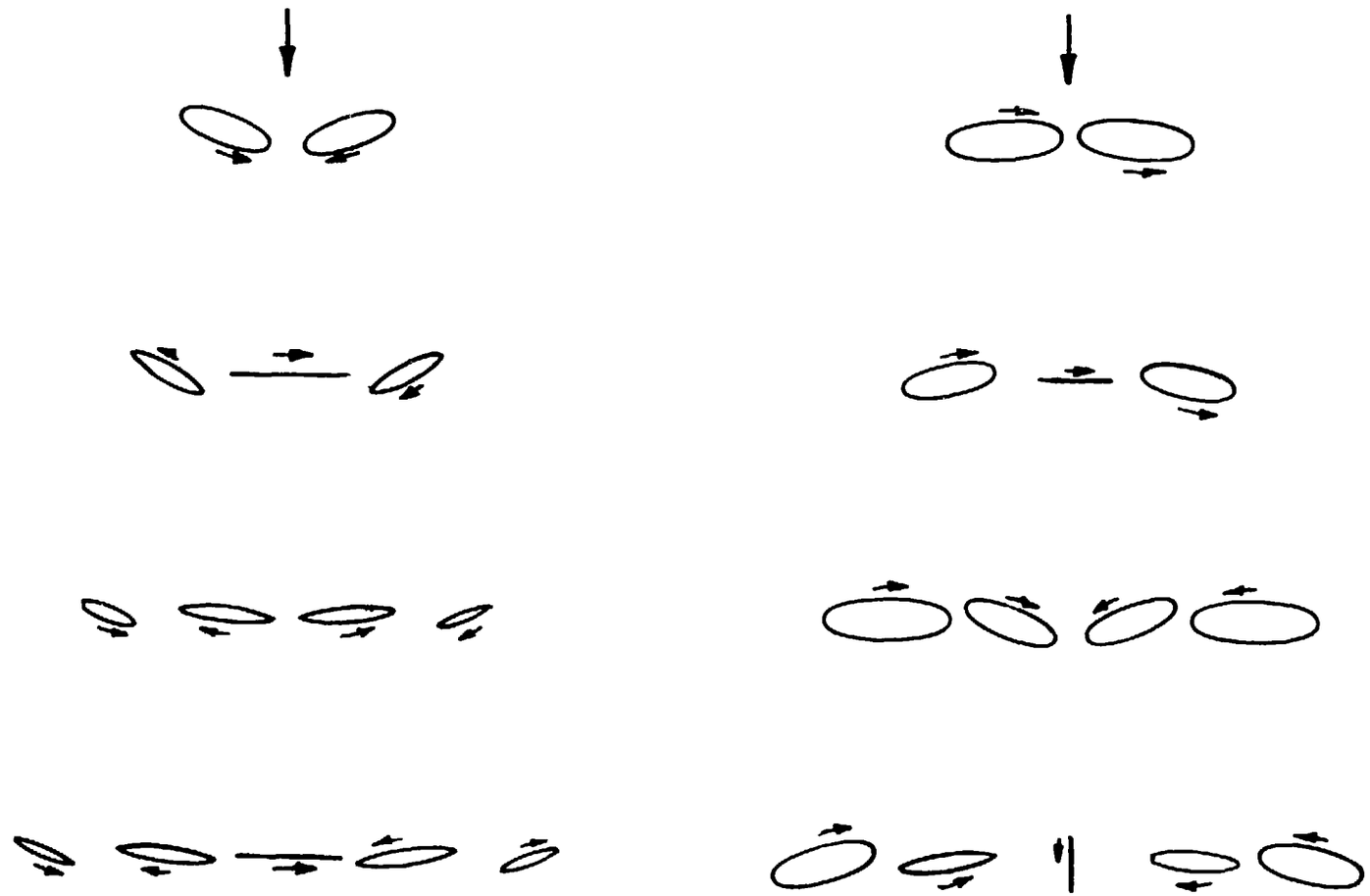

Fig. 9. Instability Modes for Tube Rows with Two, Three, Four, and Five Tubes

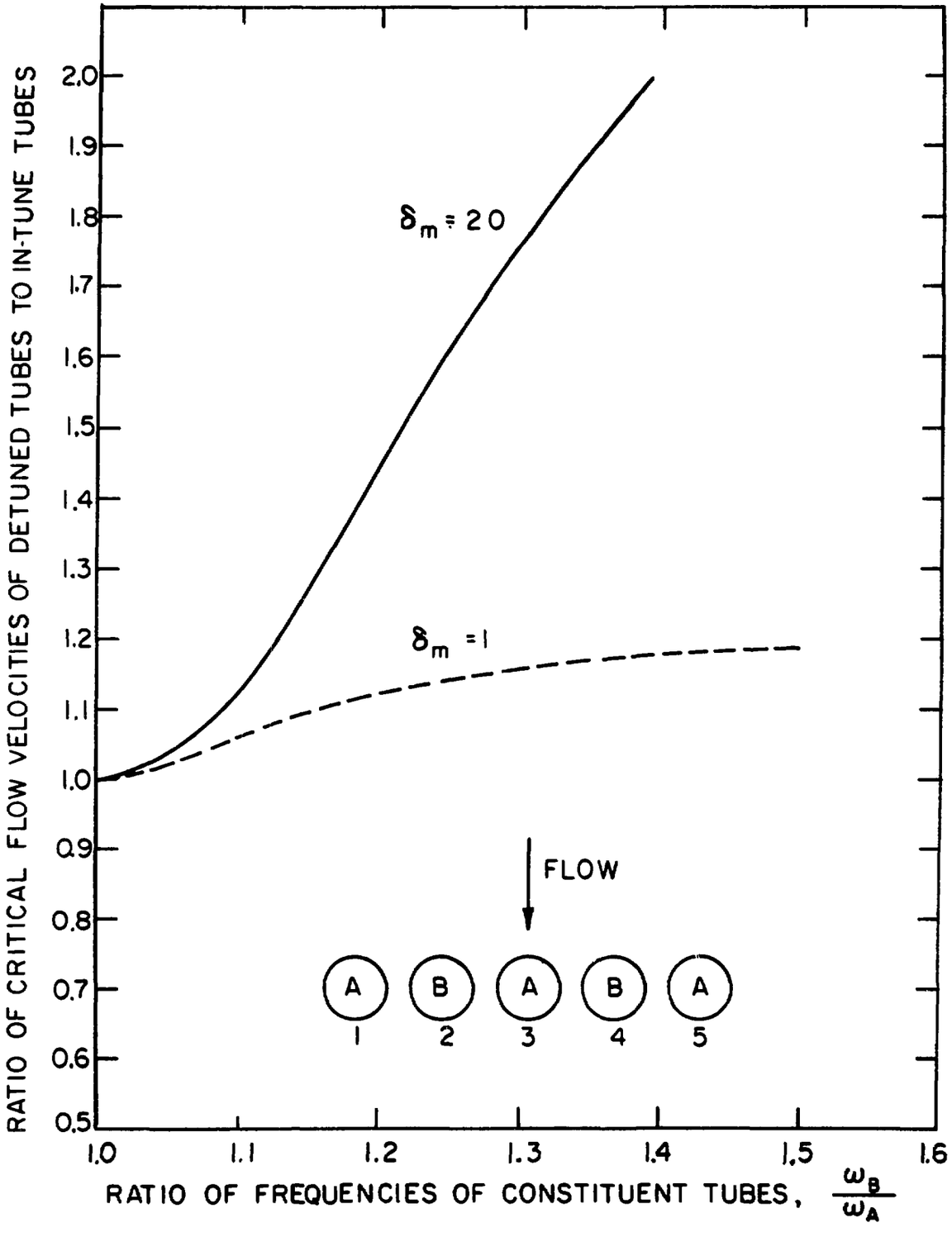

Fig. 10. Effect of Detuning in Frequency of Different Tubes on Critical Flow Velocity

for $\delta_m = 1$, the effect of detuning is not very important. The effect of detuning is much more significant in fluidelastic-stiffness-controlled instability.

Figure 11 shows the critical flow velocity of a detuned-tube row, in which natural frequencies of tube 3 in the x direction and tubes 2 and 4 in the y direction are higher, while the others are the same. In this case, detuning tends to destabilize the system. The reason for the reduction of the critical flow velocity can easily be explained. The results in Fig. 11 are calculated for $\delta_m = 40$. At this value of δ_m, the critical mode (see Fig. 9) is associated with the motion of the middle tube in the drag direction and of the two adjacent tubes in the lift direction. The detuning pattern chosen in this case coincides with the critical mode; thus, the tubes become unstable at a lower critical flow rate.

In practice, this type of detuning is probably unlikely to occur. However, this illustrates that detuning is not always beneficial. In some special situations, detuning the tubes may be detrimental.

Figure 12 shows the critical flow velocity as a function of detuning in damping. All tubes have the same natural frequencies in the two directions. However, in tubes 2 and 4, their damping value is ζ_B, while in all other tubes, their damping value is ζ_A (= 2%). The critical flow velocity is seen to increase with the damping ratio ζ_B/ζ_A. The effect of detuning in damping appears to be much smaller than that of detuning in frequency in the fluidelastic stiffness-controlled instability.

Figure 13 shows the critical flow velocities for two tube rows: one completely submerged in flow and the other with half of the tube span submerged in flow. The general shape of stability boundaries are similar, but the critical flow velocity for the partially submerged case is higher. Note that the flow velocity distribution will also affect the transition region in which the instability mechanisms switch from one to the other.

Figure 14 shows the natural frequency and modal damping ratio for an elastic tube in a rigid tube row oscillating in the lift or drag direction. Both the natural frequency and modal damping ratio are functions of the reduced flow velocity (U_m/f_vD) and mass ratio γ_v. The effect of flow on the natural frequency and modal damping ratio is much more important for heavy fluid (large γ_v). Note that when ζ_1/ζ_v is negative, the tube becomes unstable by flutter. In Fig. 14, it is seen that for $\gamma_v = 0.1$, the tube will become unstable in the lift direction in a certain range of U_m/f_vD, while for $\gamma_v = 0.01$, the tube is always stable. In the drag direction, the tube will not become unstable.

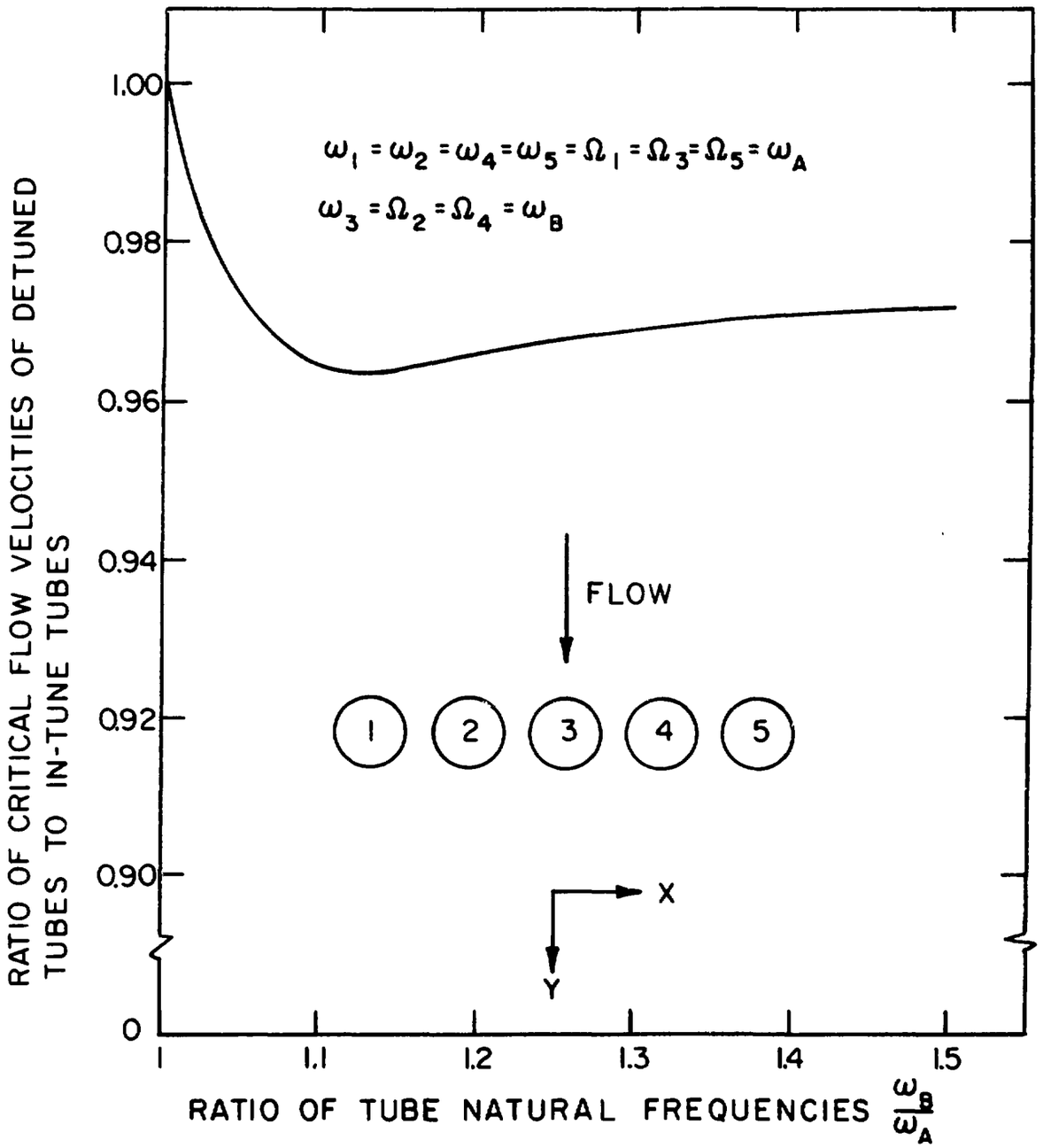

Fig. 11. Effect of Detuning in Frequency in Different Direction of Oscillation on Critical Flow Velocity

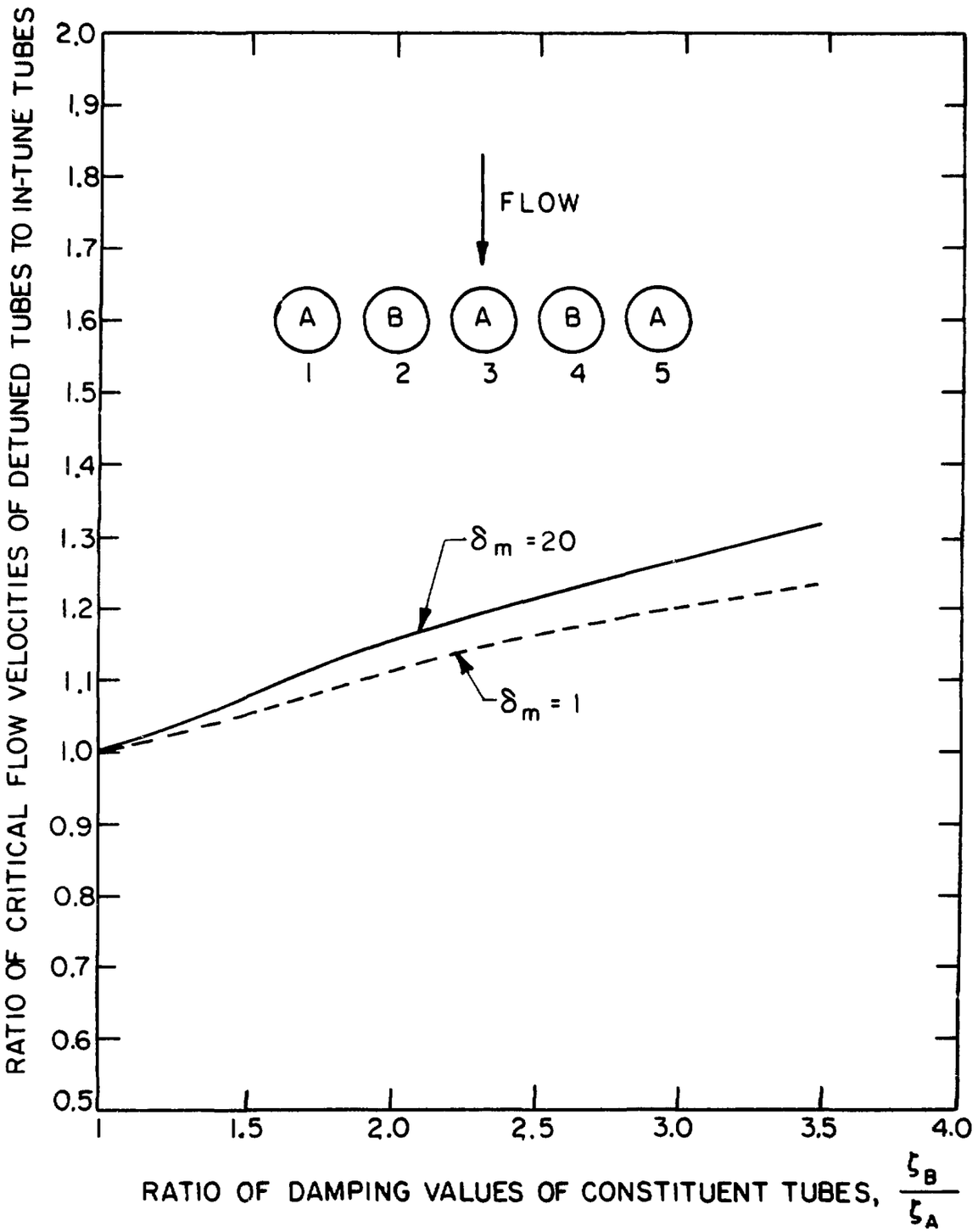

Fig. 12. Effect of Detuning in Damping on Critical Flow Velocity

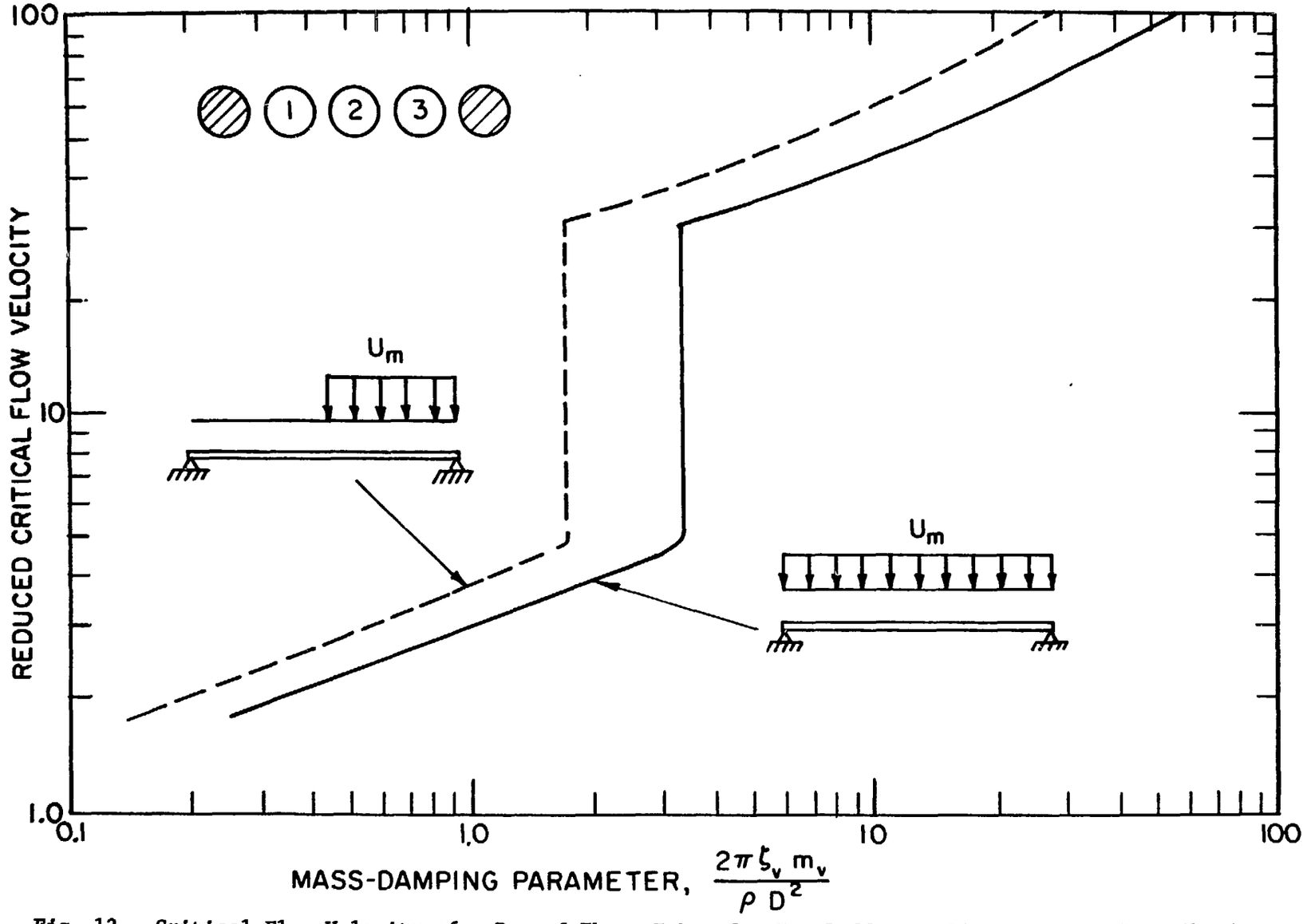

Fig. 13. Critical Flow Velocity of a Row of Three Tubes for Two Different Flow Velocity Distributions

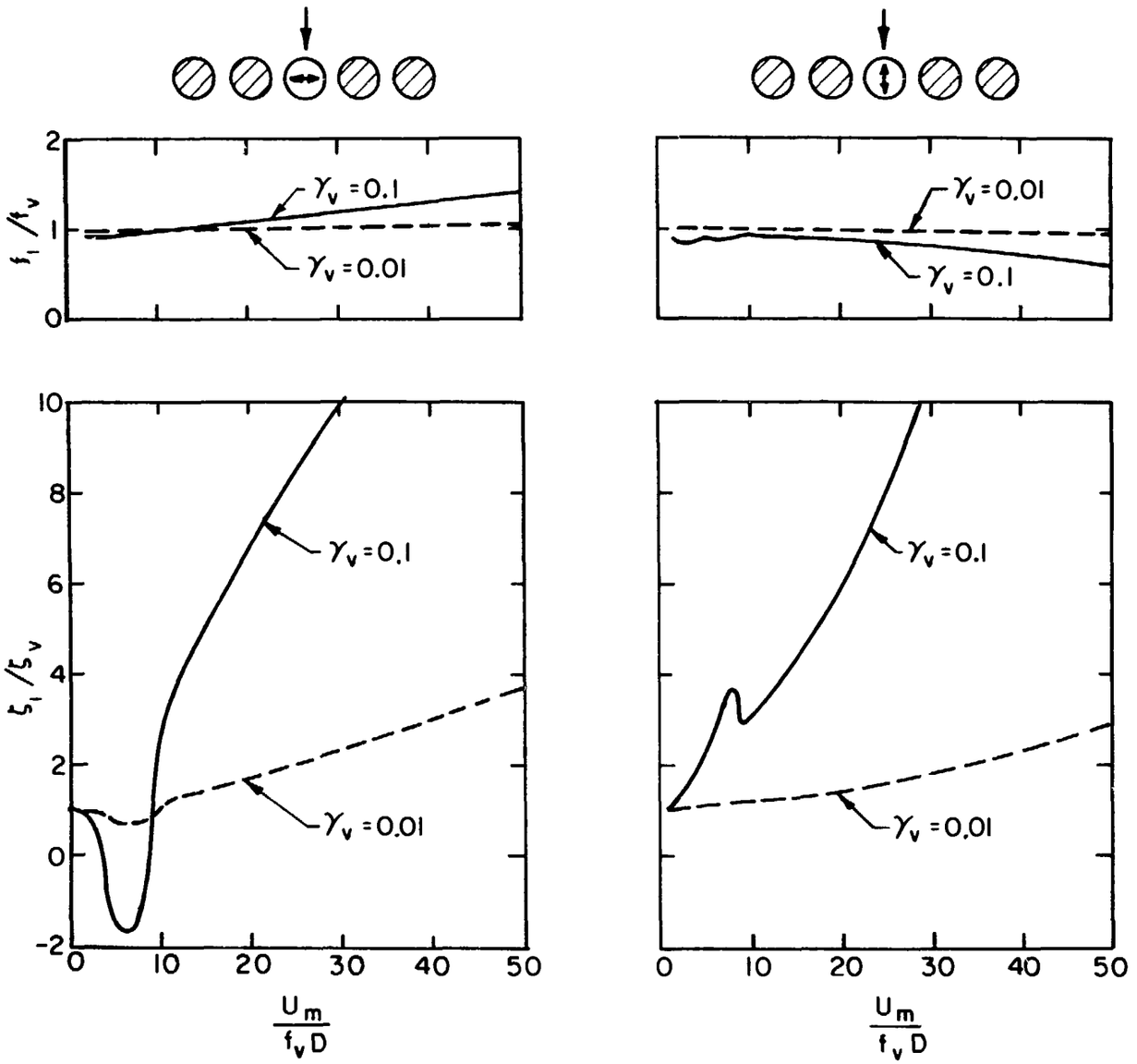

Fig. 14. Natural Frequency and Modal Damping Ratio for Constrained Modes in Flow

III. EXPERIMENT

A. Test Section

The experiments are performed in the rectangular flow channel, 10.7 cm (4.2 in.) wide and 25.9 cm (10.2 in.) high, of a test chamber connected to a water loop with a maximum flow rate of 0.052 m^3/s (700 gpm). The detail of the test chamber is the same as that used for earlier experiments for tube arrays in crossflow.[3]

Each tube element is suspended as a simply supported beam on two O-rings mounted 91.4 cm (36 in.) apart, permitting lateral vibration with equal flexibility in all directions (see Fig. 15). The O-rings are seated in the compression plates.

Three sets of brass tubes with different lengths of overhang portion ℓ_o and tube pitches are tested.

Case a

The tube outside diameter (D) is 1.59 cm (5/8 in.), the tube wall thickness is 0.318 cm (1/8 in.), the transverse pitch-to-diameter ratio is 1.35, and the overhung length is 35.6 cm. Two sequences of tests are performed: (1) all tubes are in tune, and (2) tubes 1 and 2, and tubes 4 and 5 are connected together using a rubber plug, which is pushed into the gap between the overhung ends of these tubes. These tests are referred to as Tests a.1 and a.2.

Case b

The tube outside diameter is 1.91 cm, the tube wall thickness is 0.079 cm (1/32 in.), the transverse pitch-to-diameter ratio is 1.25, and the overhung length is 25.4 cm. Three sequences of tests are performed: (1) all tubes are in tune; (2) tubes 1 and 2, and tubes 4 and 5 are connected together using a rubber plug; and (3) a weight of 66.3 grams is attached to the free ends of all tubes. These tests are referred to as Tests b.1, b.2, and b.3.

Case c

Finned tubes with an outside diameter of 1.91 cm are tested. The fin geometries of the tubes are shown in Fig. 16. The finned tubes were machined from tubes, with 19 fins per 2.54 cm. The transverse pitch-to-diameter ratio is 1.25 based on the outside diameter 1.91 cm, and the overhung length is 25.4 cm. Three sequences of tests are performed: (1) all tubes in tune; (2) tubes 1 and 2, and tubes 4 and 5 are connected together at the free ends with a rubber plug; and (3) tubes 1, 4, and 5 are

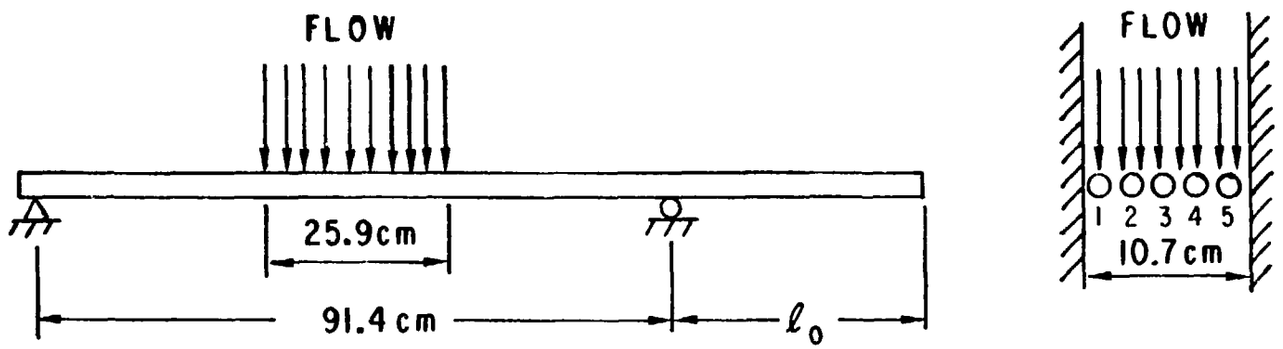

Fig. 15. Schematic of Tube Row

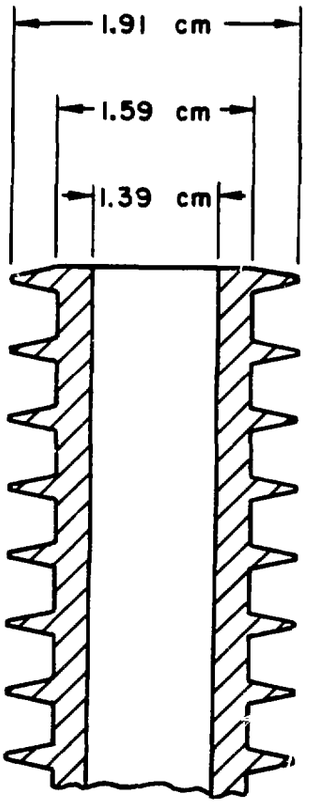

Fig. 16. Geometry for Finned Tubes

fixed at the free ends. These tests are referred to as Tests c.1, c.2, and c.3.

The different test sequences are summarized in Fig. 17. Results of these tests will give significant insight into the effects of several parameters: mass ratio of tube to fluid, damping, detuning, tube pitch, fin, and attached structural mass.

The instrumentation for the tubes consists of two accelerometers mounted at the middle of a tube with the orientation to be sensitive in the drag and lift directions. In all tests, tubes 2, 3, and 4 are instrumented with two accelerometers. The accelerometers are installed by means of a small mounting block attached to the inside of the tubes and the leads brought to the outside. The tube-accelerometer outputs are amplified by charge amplifiers and coupled to double-integration circuits and an analog tape recorder. Displacement signals obtained from the double integrators are then analyzed using the FFT analyzer.

B. Test Procedures

Tests for each test are made in air, still fluid, and flowing fluid.

1. Air Environment

Testing in air is performed to determine the natural frequency and damping of each instrumented tube. The tube is excited by plucking it at the free end. The transient response of the tube is recorded. Then, the damping is obtained from the log decrement of the displacement trace, and the natural frequency is determined from the power spectrum of the displacement. Each instrumented tube is tested in two orthogonal directions.

2. Still Fluid

Uncoupled natural frequency and modal damping ratio are determined using the same procedure as in air. In this test, all the tubes surrounding the tubes being tested are held at the overhung end by hands to eliminate responses of those tubes.

3. Flowing Fluid

The flow velocity is increased at small intervals. At each flow velocity, the displacement signals in the lift and drag directions are recorded on a magnetic tape for several minutes for subsequent analysis. The test is terminated when tube impact occurs.

In some test cases, such as Test a.1, there are multiple stable and unstable regions. The flow velocity is increased rapidly to reach to the second stable region. Then, the flow is decreased or increased at small intervals to determine the lower and upper stability boundaries.

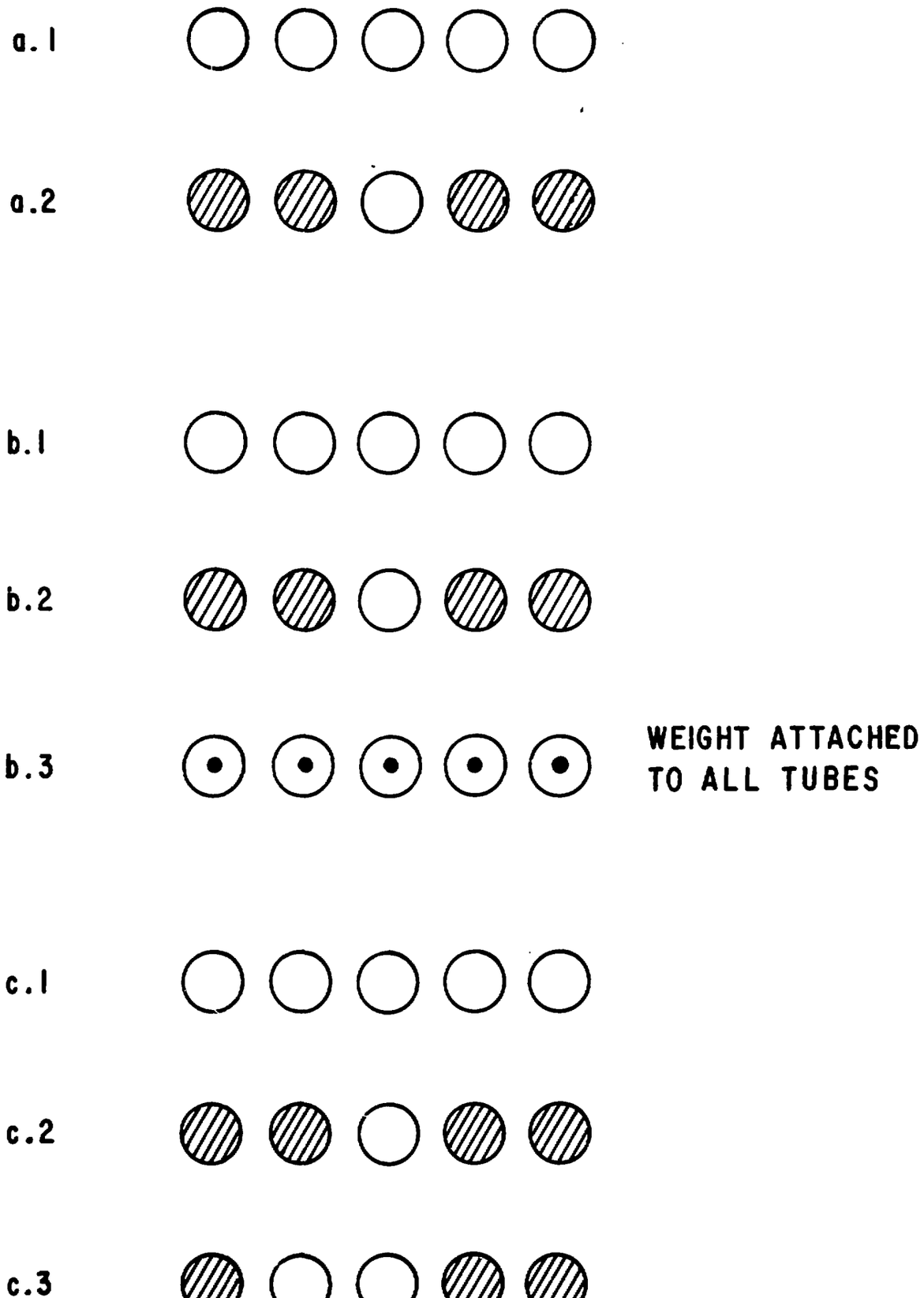

Fig. 17. Different Test Cases

Tube damping depends on water temperature; this is attributed to O-rings, whose characteristics are a function of temperature. Therefore, tube damping can be controlled by controlling water temperature. In each test sequence, the tube row is tested under several different temperatures: in-air test at room temperature, and in-fluid and in-flow tests at several loop temperatures with one of them being equal to room temperature.

C. Experimental Data

Case a

Figures 18 and 19 show the natural frequency and modal damping ratio as functions of temperature. The variation of natural frequencies with temperature is small, but damping varies significantly with temperature.

Figures 20-22 show typical tube displacements as functions of flow velocity for several temperatures. The displacement component in the lift direction is denoted by T, and in the drag direction by I; e.g., 2T denotes the displacement component of tube 2 in the lift direction.

For $U_m < U_1$ (see Figs. 20-22), the tube displacements are very small. As U_m is increased to U_1, the tubes become unstable. Therefore U_1 is the lowest critical flow velocity. At U_1, the tube vibration amplitude increases rather slowly. If the flow velocity is increased rapidly from a value less than U_1 to that above U_2, the tubes will not become unstable. However, if the flow velocity is decreased to U_2, large tube motions occur. The increase of oscillation amplitude at U_2 is much more rapid than that at U_1. For $U_1 < U_m < U_2$, tubes are unstable; in this region, tubes may impact with one another. For $U_m > U_2$, although tube motions may be relatively large, the tubes in general do not impact with the neighbor tubes. In most cases, the tubes move in phase for $U_m > U_2$. In some cases, the tubes may become unstable at one of its higher modes. Once the tubes lose stability at a higher frequency, the large tube motion will cause impact of neighbor tubes and one of the lower-frequency modes will be dominant again.

Figures 23 and 24 show the frequency spectra of tube displacements at various flow velocities at two different temperatures. At high temperature, the frequency spectra contain a sharp peak. At low temperature, the frequency spectra for U_m larger than U_2 are broad band. Note that, in some cases, there is a shift in the dominant frequency at U_1 and U_2.

The results of Tests a.1 and a.2 are summarized in Table 1. There are two critical flow velocities in Test a.1, which correspond to the lower and upper bounds of the first unstable region.

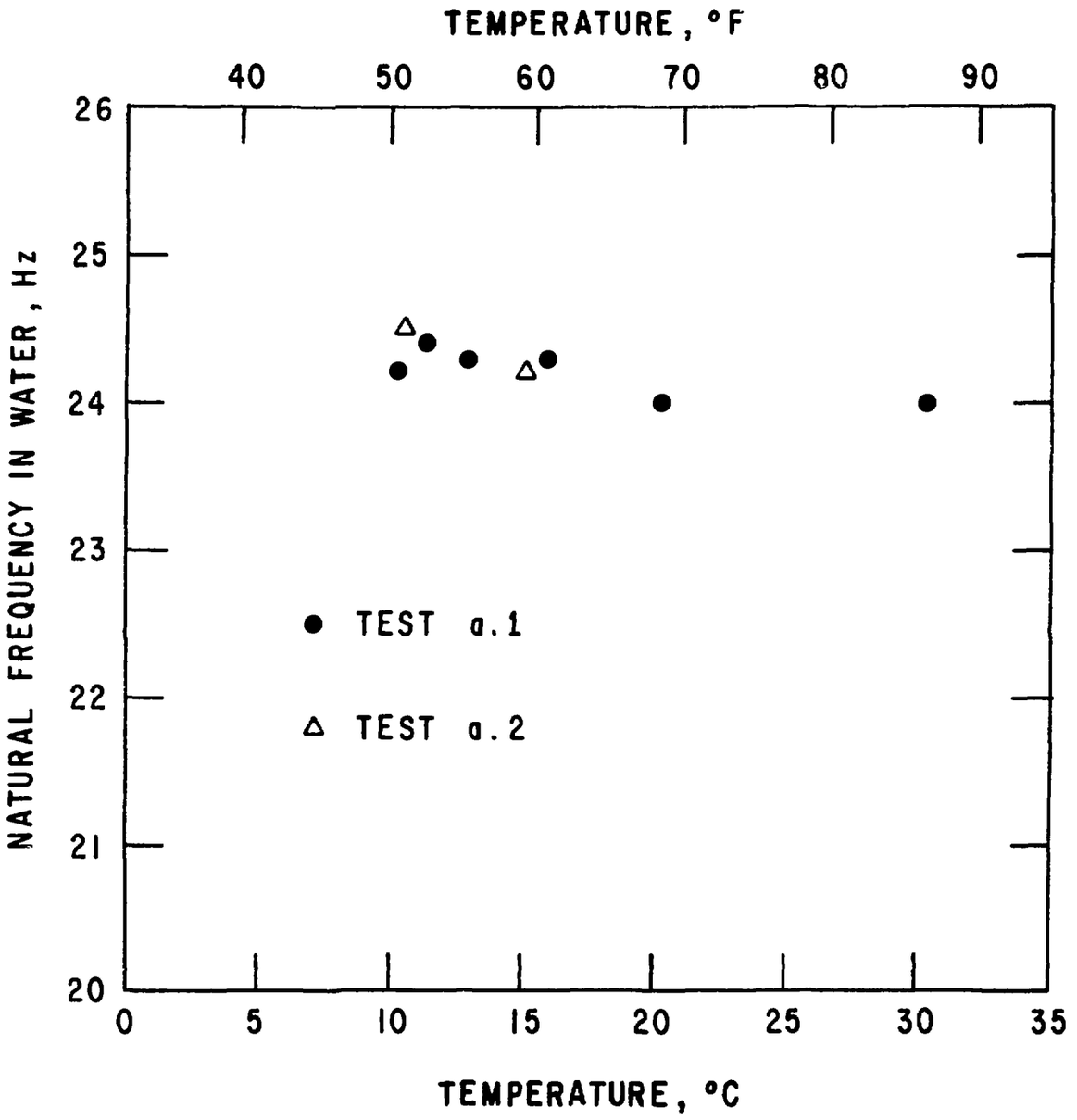

Fig. 18. Natural Frequencies in Water for Tests a.1 and a.2

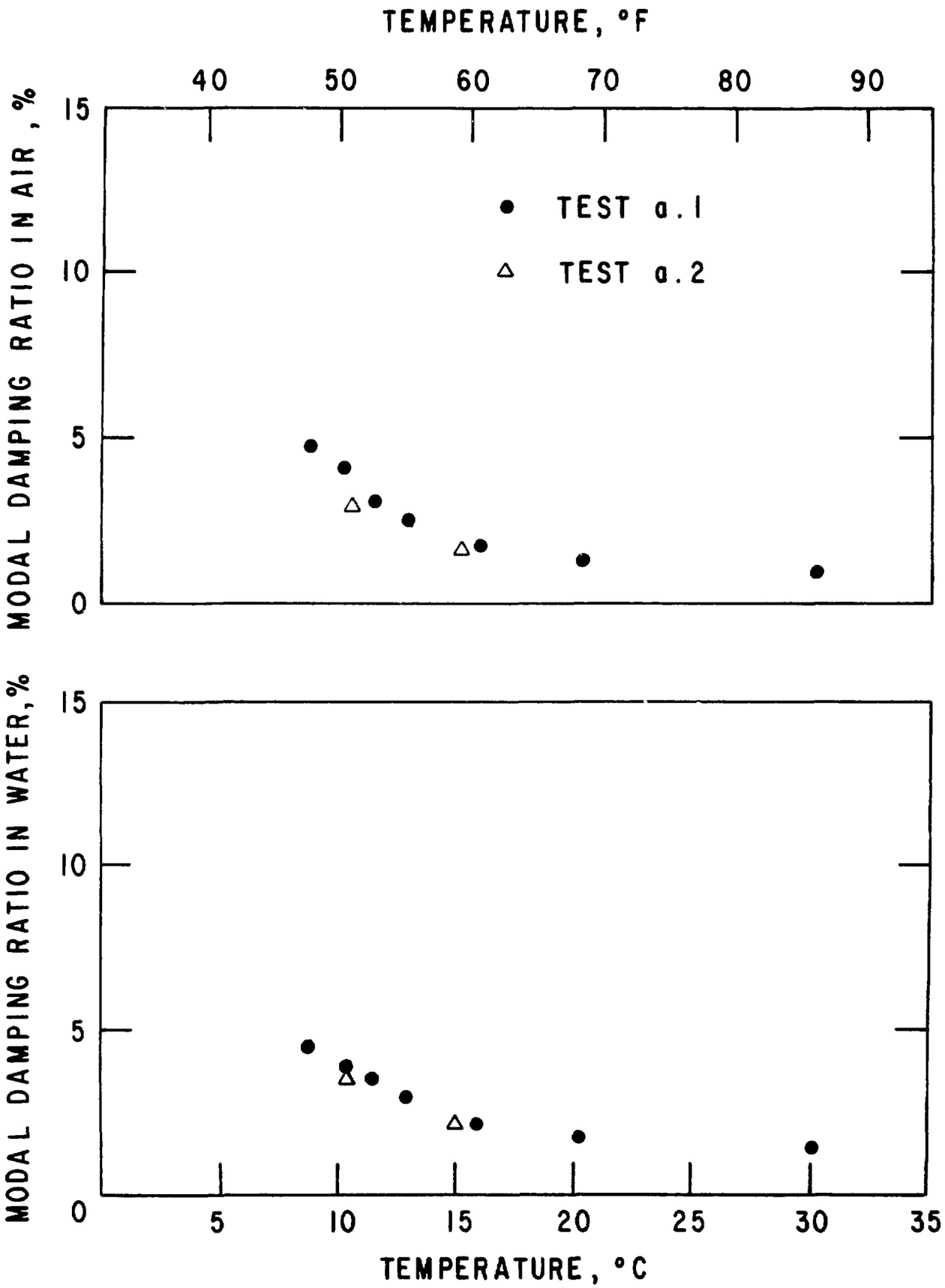

Fig. 19. Modal Damping Ratio in Air and in Water for Tests a.1 and a.2

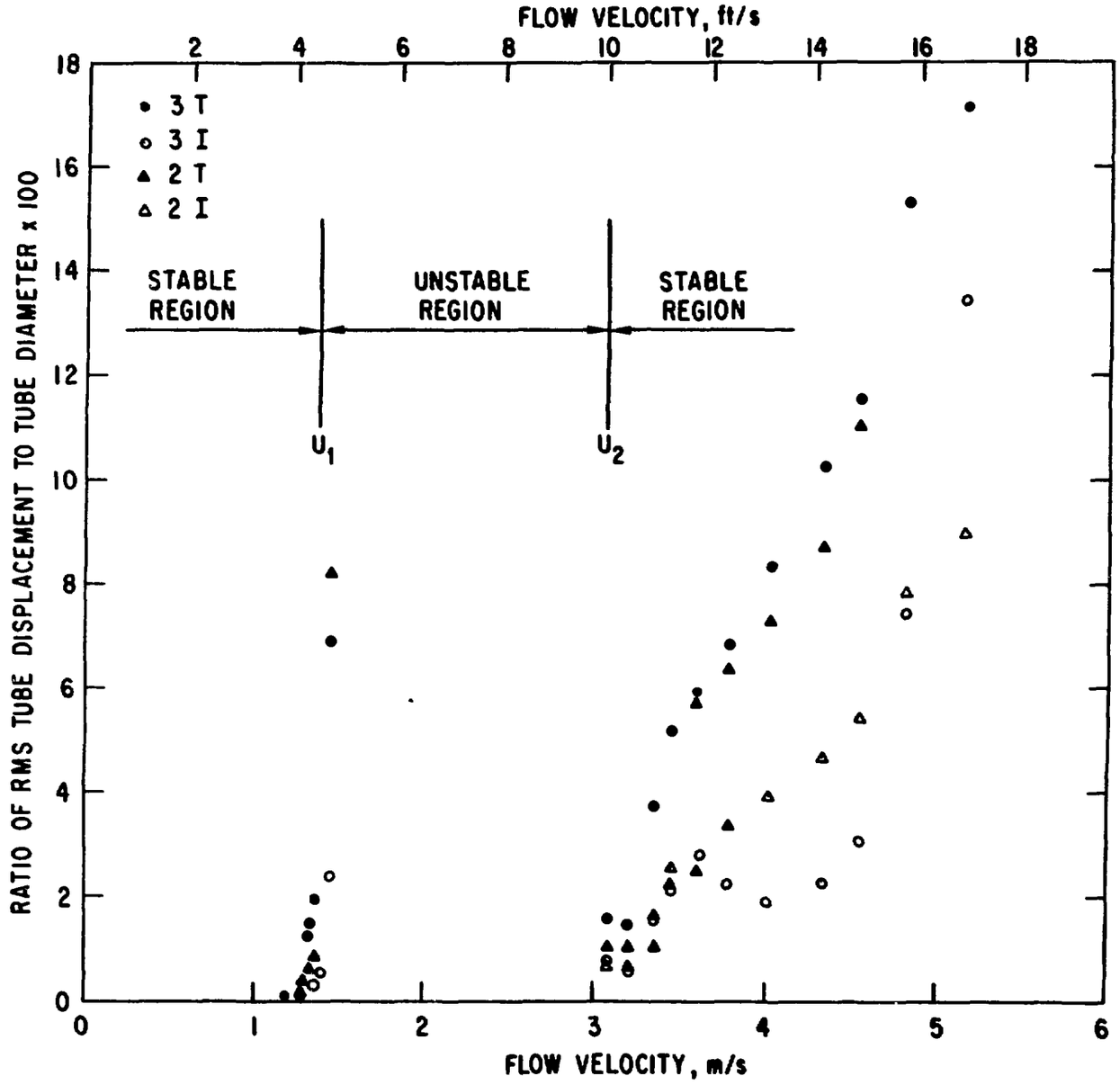

Fig. 20. Tube Displacement as a Function of Flow Velocity in Test a.1 at 15.89°C

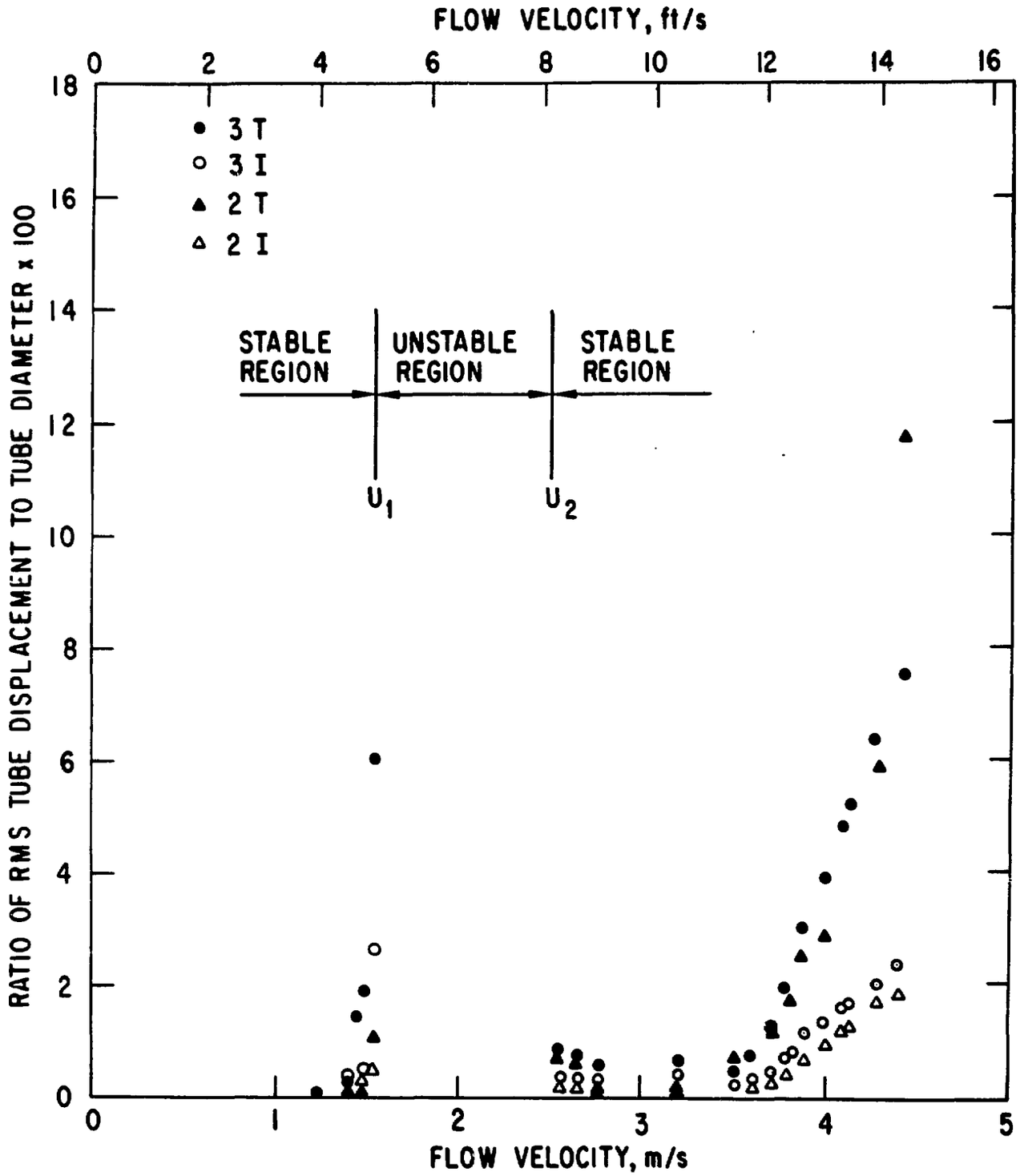

Fig. 21. Tube Displacement as a Function of Flow Velocity in Test a.1 at 11.44°C

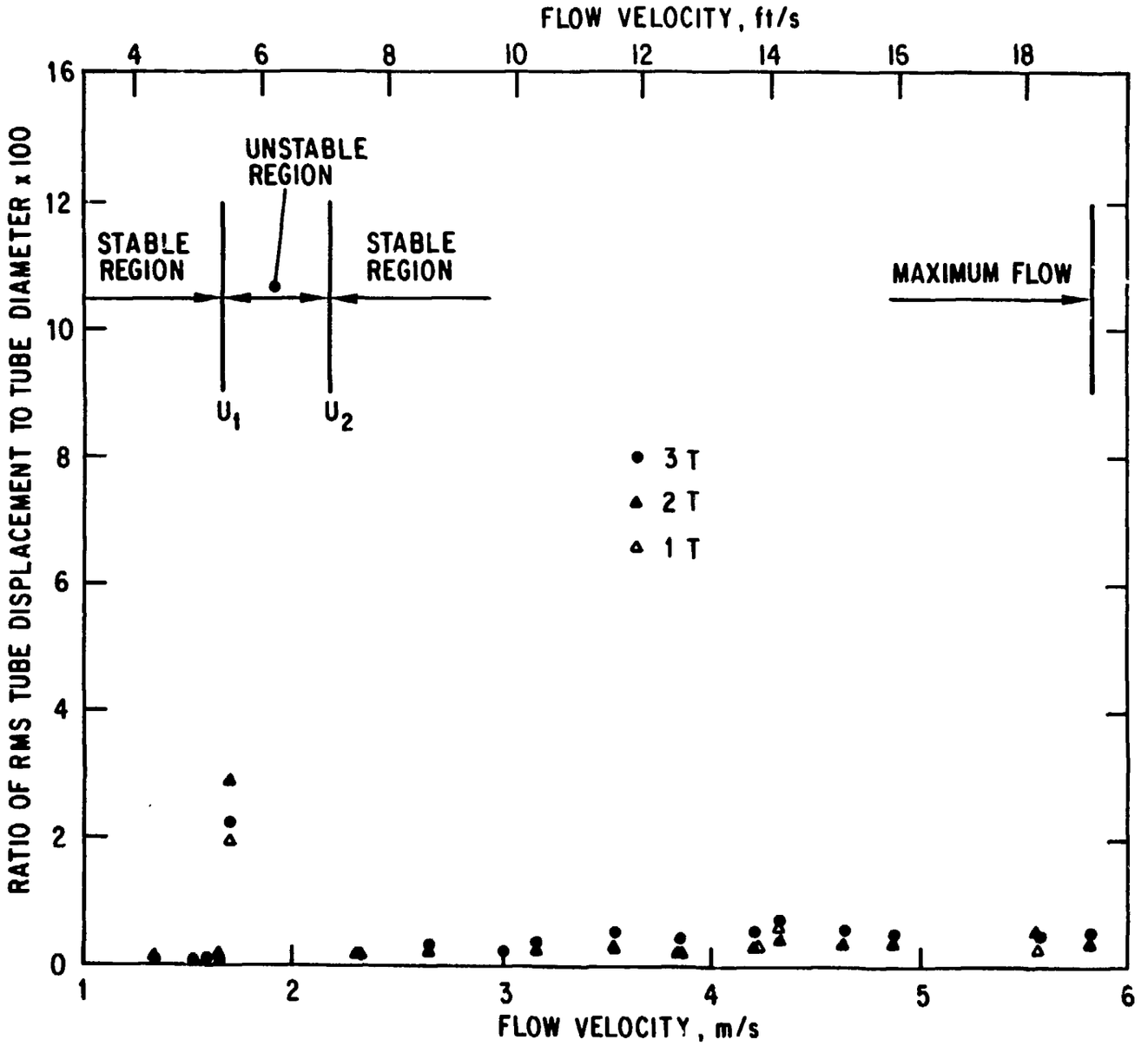

Fig. 22. Tube Displacement as a Function of Flow Velocity in Test a.1 at 8.78°C

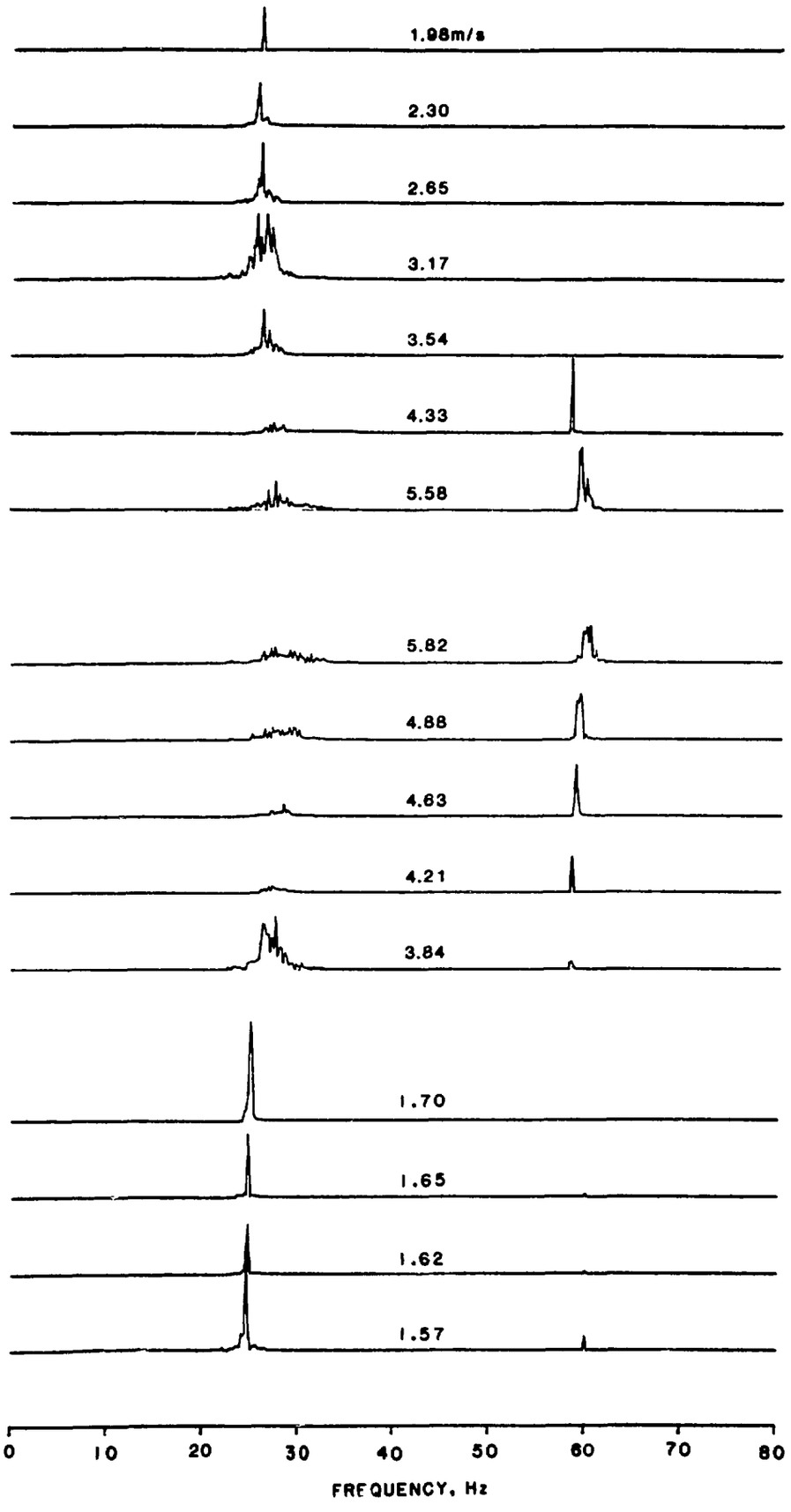
1.98m/s
2.30
2.65
3.17
3.54
4.33
5.58
5.82
4.88
4.63
4.21
3.84
1.70
1.65
1.62
1.57
0
10
20
30
40
50
60
70
80
FREQUENCY, Hz

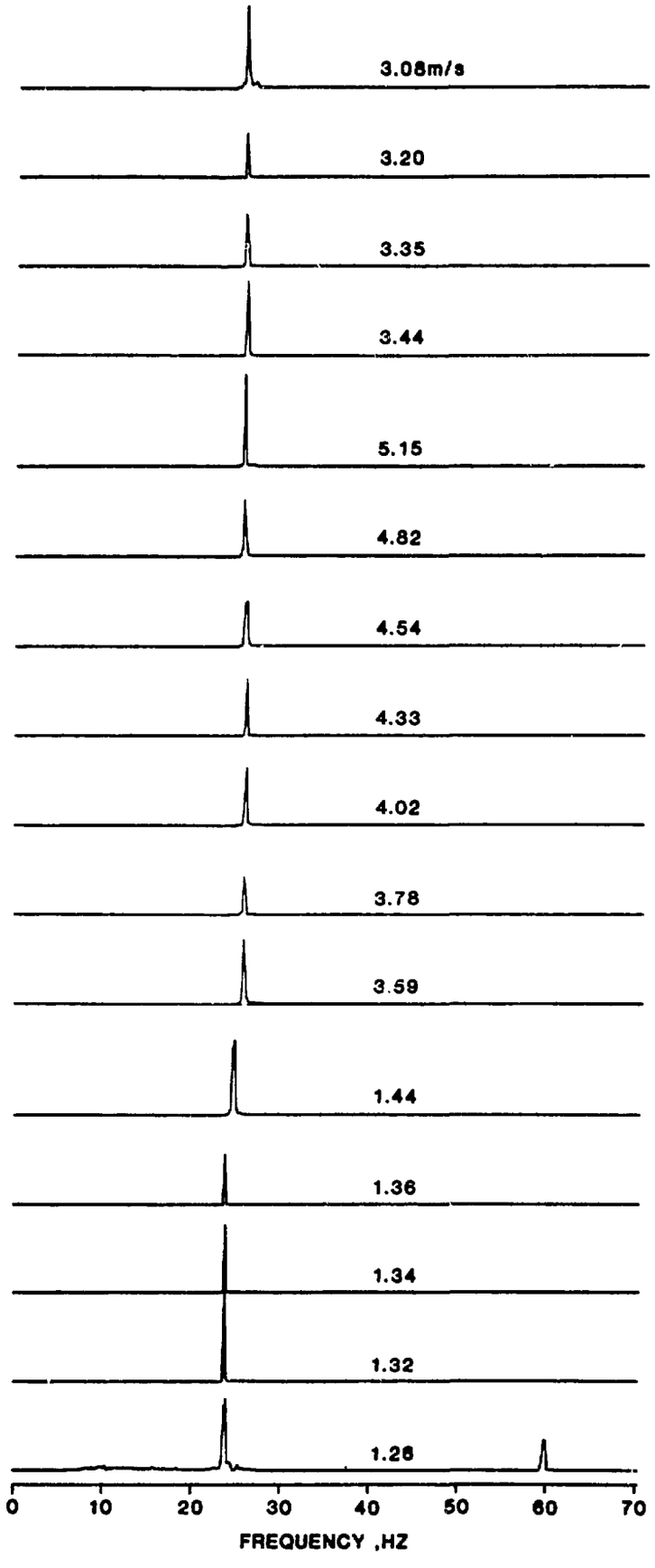

Fig. 24. Frequency Spectra of Tube Displacements of Tube 3 in the Lift Direction in Test a.1 at 15.89°C

Table 1. Experimental Data for Tests a.1 and a.2

Test	Temperature, °C	Natural Frequency, Hz		Modal Damping Ratio, %		Oscillation Frequency at Instability, Hz	Critical Flow Velocity, m/s	$\frac{U_m}{f_v D}$	$\frac{2\pi m_v \zeta_v}{\rho D^2}$
		In Air	In Water	In Air	In Water				
a.1	8.78	26.1	24.5	4.5	4.8	25.0 26.0	1.68 2.19	4.05 5.29	1.13
	10.39	26.1	24.2	3.8	4.1	24.2 26.0	1.52 2.26	3.68 5.44	0.96
	11.44	26.3	24.4	3.1	3.5	24.1 25.5	1.44 2.53	3.46 6.14	0.78
	13.00	26.2	24.3	2.6	3.0	24.0 25.5	1.37 2.73	3.30 6.56	0.65
	15.89	26.2	24.3	1.7	2.1	23.9 25.5	1.29 3.08	3.11 7.40	0.43
	20.28	25.9	24.0	1.2	1.7	23.6 25.0	1.26 3.38	3.05 8.23	0.30
	30.17	25.9	24.0	0.9	1.4	23.5	1.14	2.78	0.23
a.2	7.33	26.7	24.8	3.9	4.2	38.4[a]	2.30		
	12.22	26.4	24.5	2.9	3.3	38.4[a]	2.14		
	15.17	26.1	24.8	1.6	2.0	24.3	1.54	3.71	0.40

[a]Instability associated with tubes 1 and 2 or 4 and 5 at a higher-frequency mode.

In Test a.2, at 15.17°C, the instability is associated with tube 3. However, at the other two temperatures, it is associated with the other four tubes with higher frequencies.

Case b

Figures 25 and 26 show the natural frequency and modal damping ratio. Results of Tests b.1 and b.2 agree well. The attached weight at the free end (Test b.3) reduces the natural frequency, but it does not affect the modal damping value.

Figures 27 and 28 show typical tube displacements as functions of flow velocity. At higher temperature, the tubes become unstable. However, at low temperature the tubes do not lose stability for flow velocity up to about 5.5 m/s.

Figures 29 and 30 show typical frequency spectra of tube displacements. At 23.61°C for Test b.3, the tubes respond predominantly at a single frequency. As the flow velocity is increased from 1.70 to 1.71 m/s, the frequency is shifted to another frequency, which is the frequency of the critical mode. At 1.71 m/s, the tubes become unstable. At 4.94°C for Test b.3, the frequency spectra are more widely spread. For flow velocity up to 5.52 m/s, the tubes do not become unstable.

Test results for Cases b.1, b.2, and b.3 are summarized in Table 2.

Case b.1. The critical flow velocity ($U_m/f_v D$) increases with δ_m. The instability mode does not vary with temperature (damping).

Case b.2. At 15.89 and 23.50°C, tube 3 loses stability, while the other tubes remain stable. The oscillation frequencies at instability are 33.8 and 32.9 Hz. At 4.83°C, the tubes become unstable due to tubes 1, 2, 4, and 5, and the oscillation frequency is 49.5 Hz.

Case b.3. For temperature higher than 6.83°C, the instability is of fluid-damping-controlled type. There is a jump in the critical flow velocity at a temperature near 6.83°C. The data for 4.78, 4.94, and 6.11°C are nondimensionalized using the natural frequency of the first mode. No detailed results of the response characteristics are measured, since the tubes impact with one another. However, from the limited frequency spectra at these temperatures, the instability is associated with the higher modes.

Case c

Figures 31 and 32 show the natural frequencies and modal damping ratio. The results of various tests agree reasonably well.

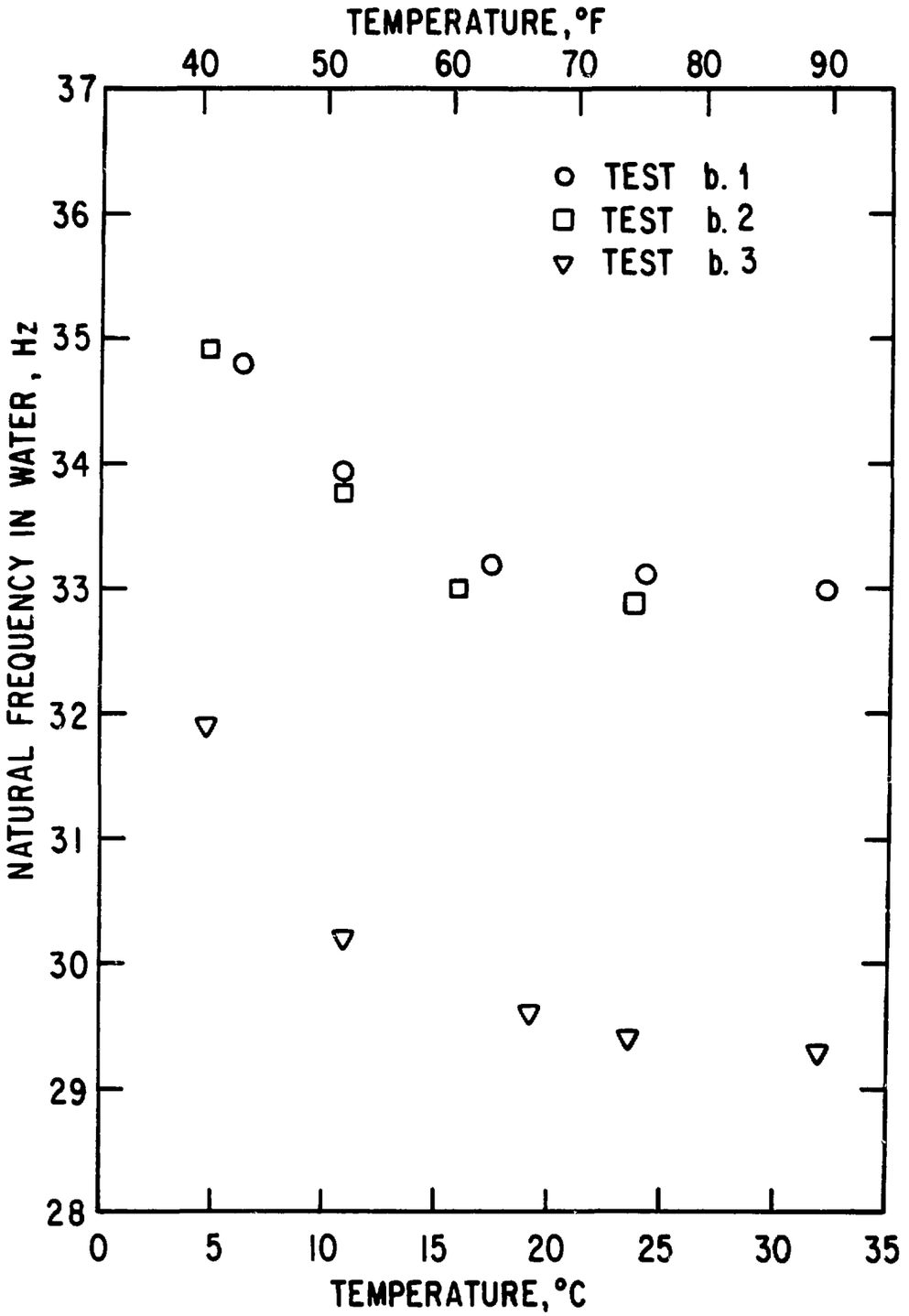

Fig. 25. Natural Frequencies in Water for Tests b.1, b.2, and b.3

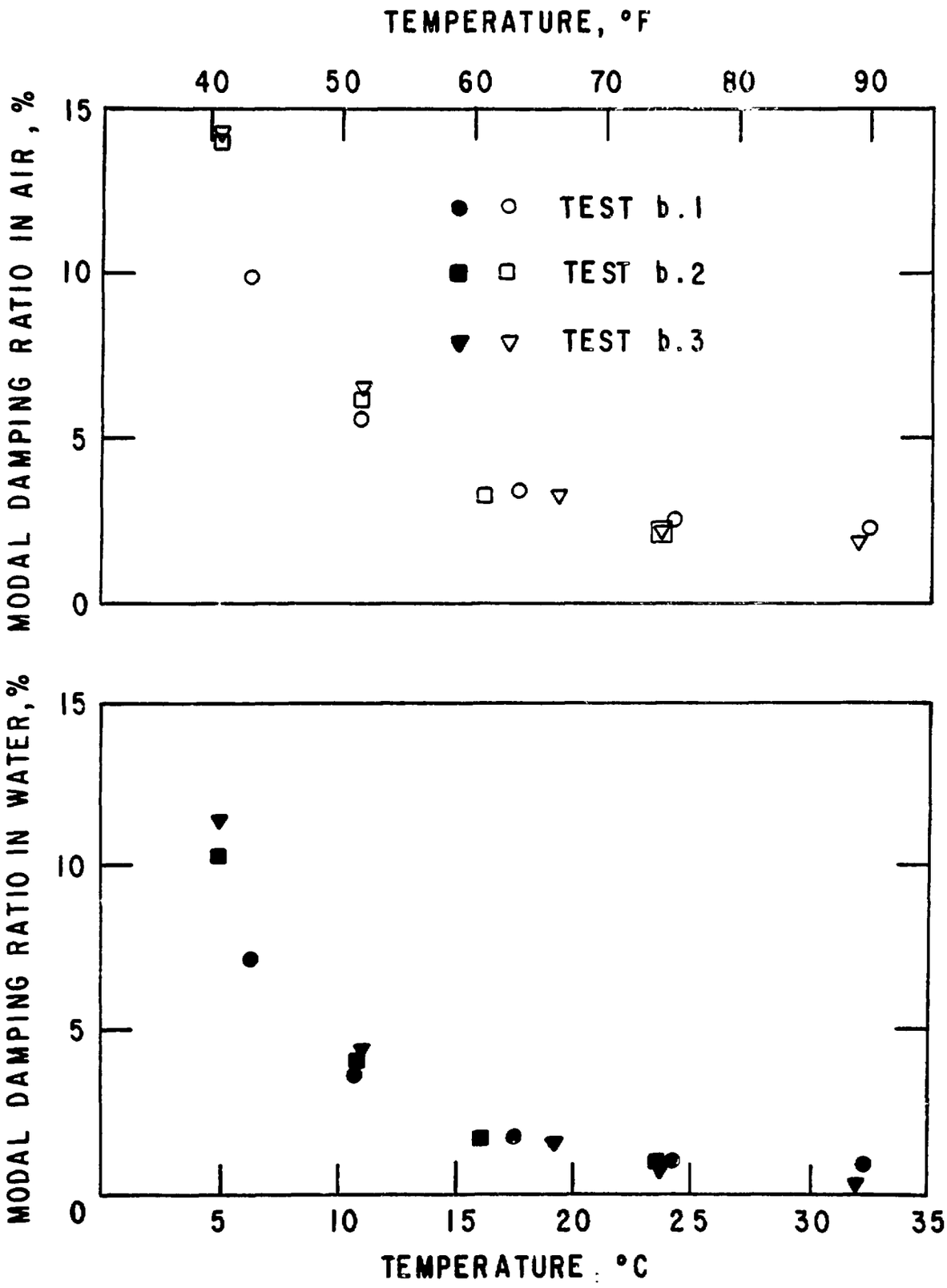

Fig. 26. Modal Damping Ratios in Air and in Water for Tests b.1, b.2, and b.3

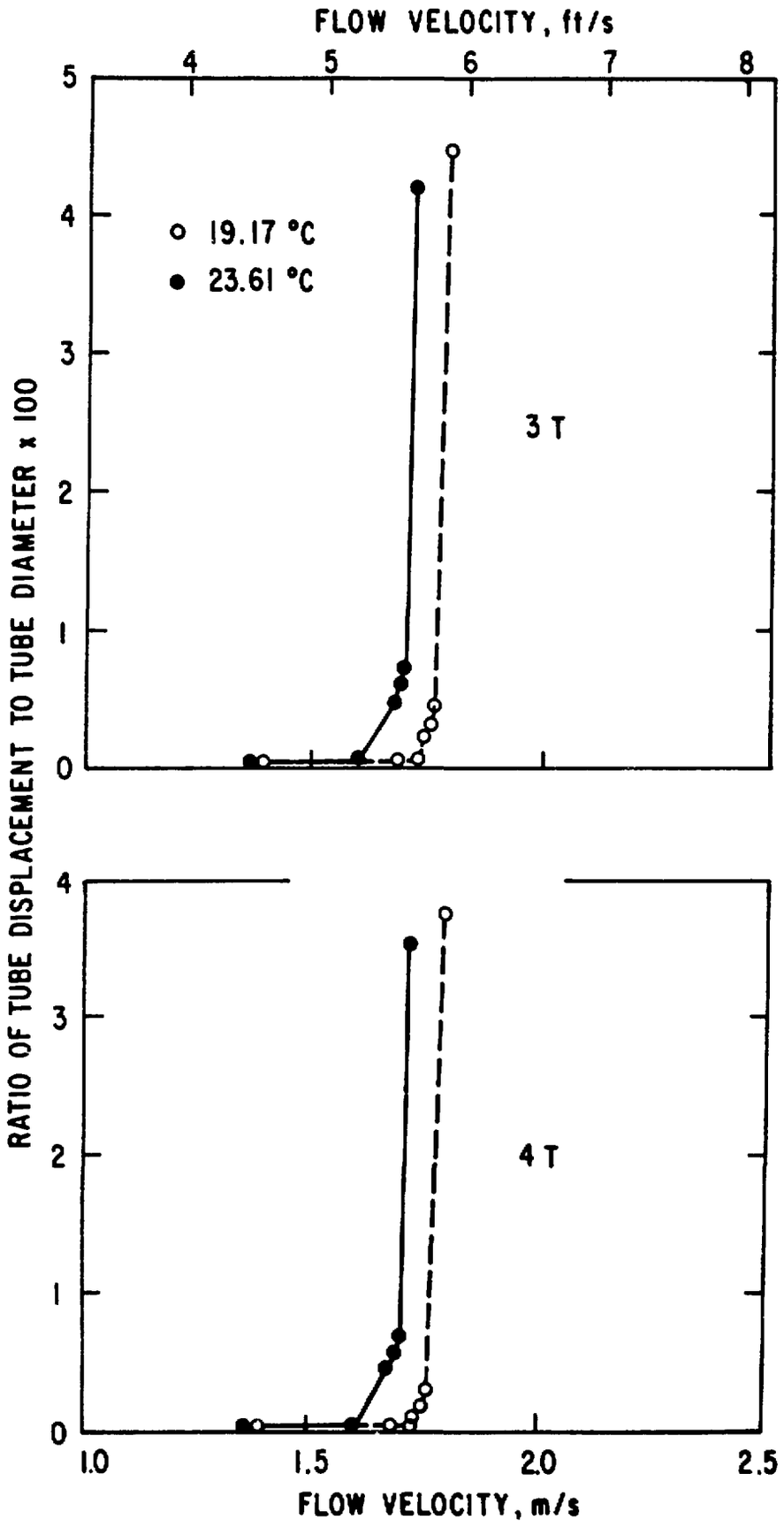

Fig. 27. Tube Displacements of Tubes 2 and 3 in the Lift Direction in Test b.3 at 19.17 and 23.61°C

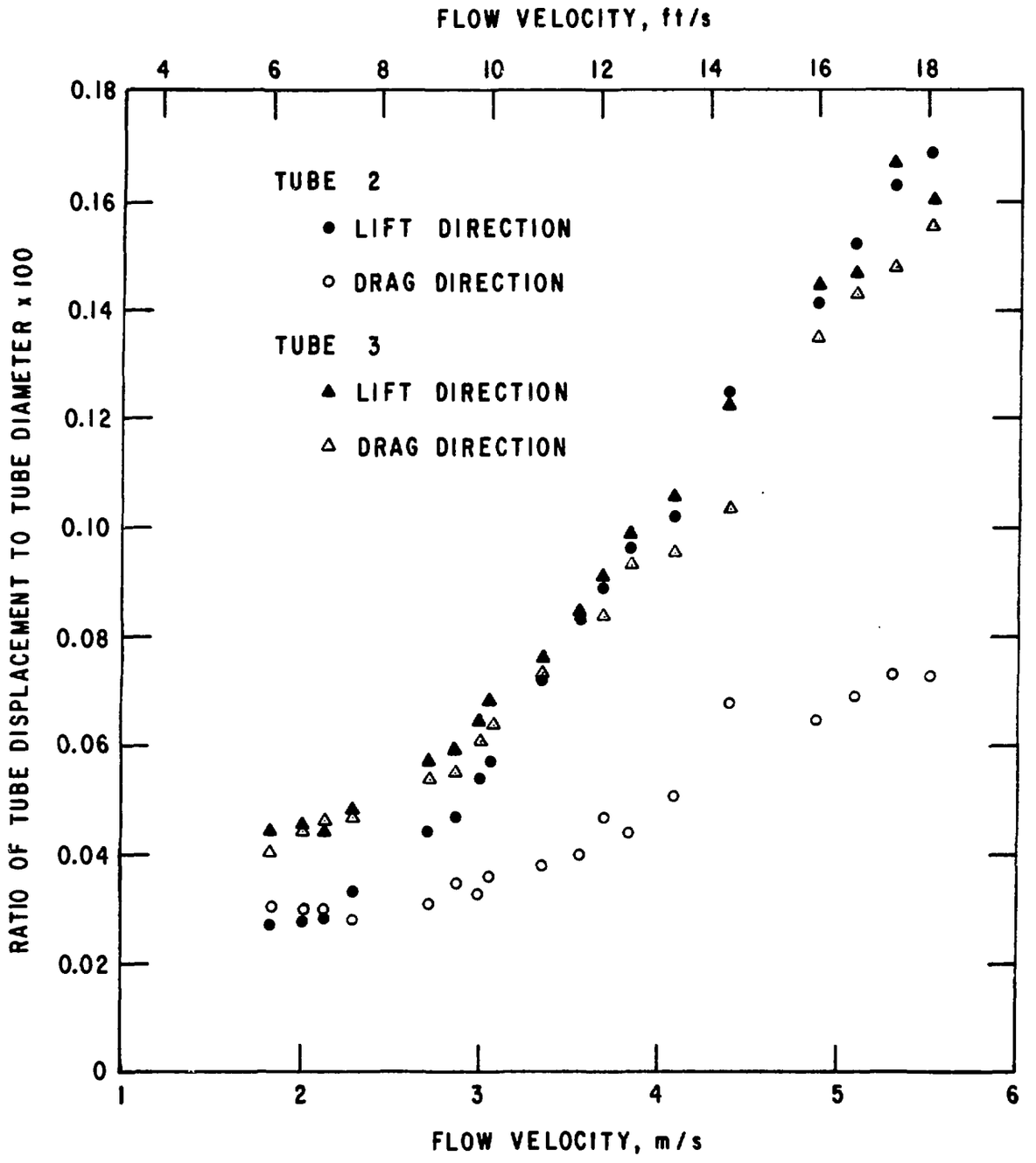

Fig. 28. Tube Displacements of Tubes 2 and 3 in Test b.3 at 4.94°C

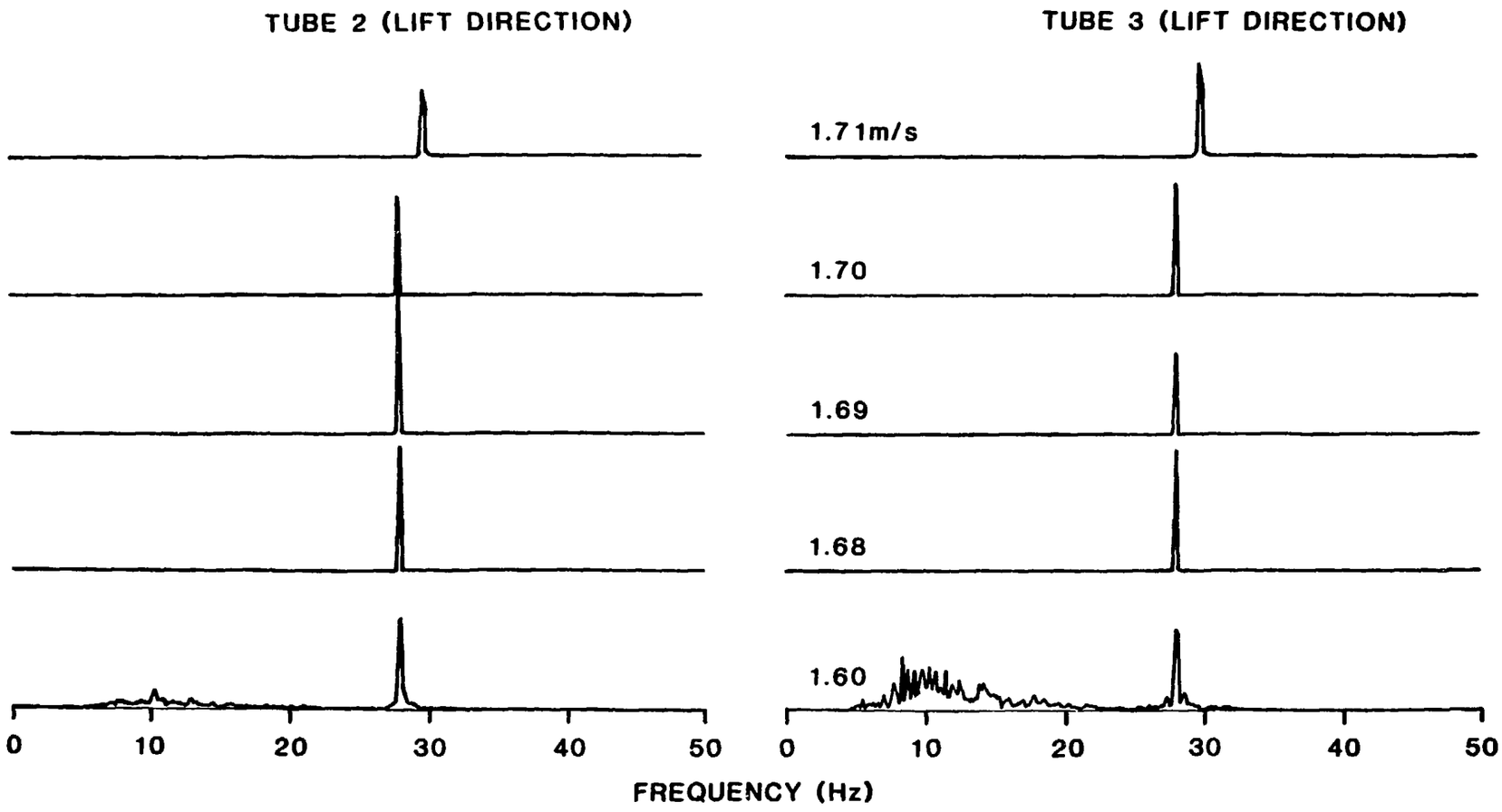

Fig. 29. Frequency Spectra of Tube Displacement of Tubes 2 and 3 in the Lift Direction in Test b.3 at 23.61°C

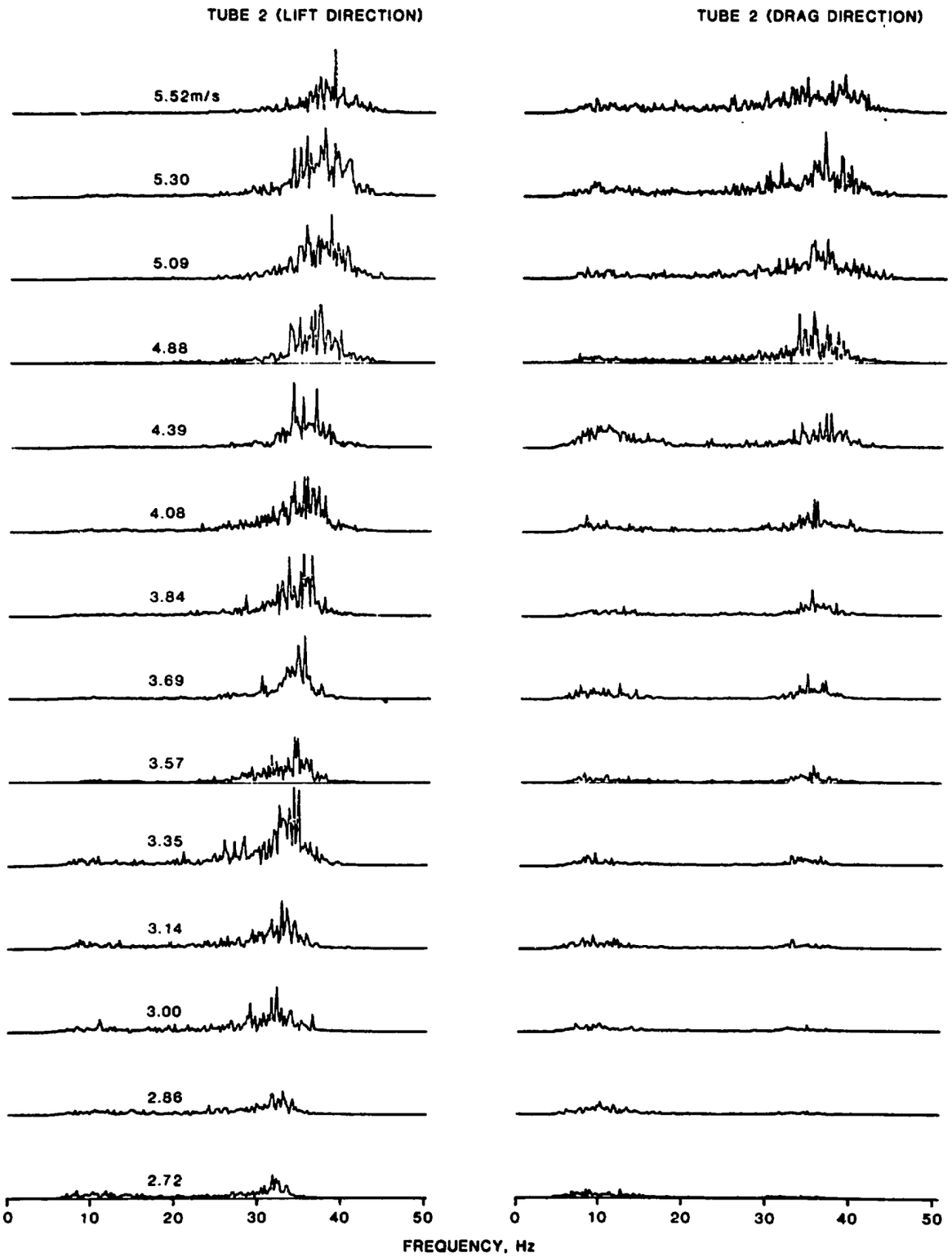

Fig. 30. Frequency Spectra of Tube Displacement of Tube 2 in Test b.3 at 4.94°C

Table 2. Experimental Data for Tests b.1, b.2, and b.3

Test	Temperature, °C	Natural Frequency, Hz		Modal Damping Ratio, %		Oscillation Frequency at Instability, Hz	Critical Flow Velocity, m/s	$\frac{U_m}{f_v D}$	$\frac{2\pi m_v \zeta_v}{\rho D^2}$
		In Air	In Water	In Air	In Water				
	6.28	42.8	34.8	10.0	9.2	34.2	2.66	3.25	1.04
	10.78	41.8	33.9	5.6	5.7	32.0	2.14	2.69	0.59
b.1	17.44	40.9	33.2	3.4	3.9	31.0	1.92	2.46	0.35
	24.00	40.8	33.1	2.5	3.1	30.8	1.81	2.33	0.26
	32.22	40.7	33.0	2.3	3.0	30.7	1.76	2.28	0.24
	4.83	43.0	34.9	14.0	12.4	49.5[a]	3.75		
b.2	15.89	40.7	33.0	6.3	3.8	33.8	2.53	3.04	0.34
	23.50	40.5	32.9	2.3	2.9	32.9	1.94	2.51	0.24
	4.78	36.1		15.2			5.50	8.12	2.39
	4.94	36.0	31.9	14.4	13.6		5.70	8.31	2.26
	6.11	35.4		10.8			5.64	8.36	1.70
	6.83	35.1		9.6			2.99	4.47	1.51
b.3	7.78	34.8		8.3			2.59	3.91	1.31
	11.00	34.1	30.2	6.5	6.5	29.0	2.02	3.11	1.03
	19.17	33.4	29.6	3.3	3.7	29.9	1.78	2.79	0.52
	23.61	33.2	29.4	2.3	2.7	29.8	1.70	2.70	0.35
	31.83	33.1	29.3	1.9	2.4	30.2	1.63	2.58	0.30

[a]At this temperature, the oscillation frequency at instability is much higher than the other temperatures; the instability mode is associated predominantly with the motion of tubes 1, 2, 4, and 5.

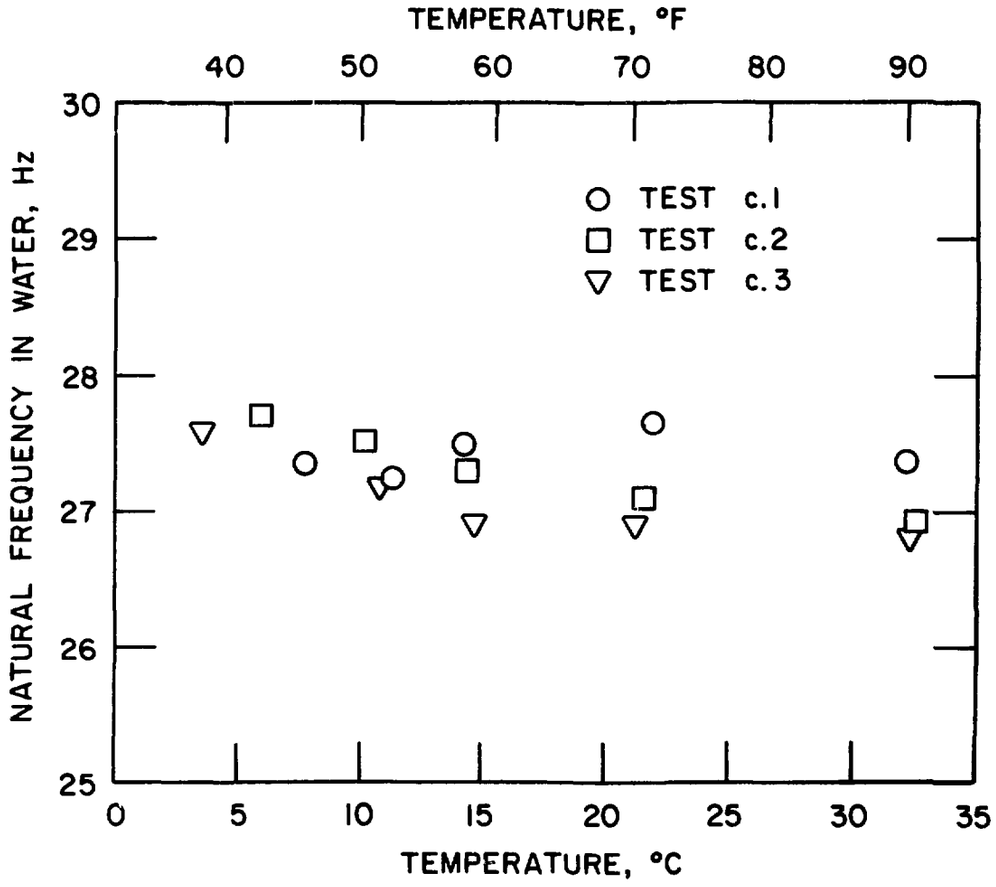

Fig. 31. Natural Frequencies in Water for Tests c.1, c.2, and c.3

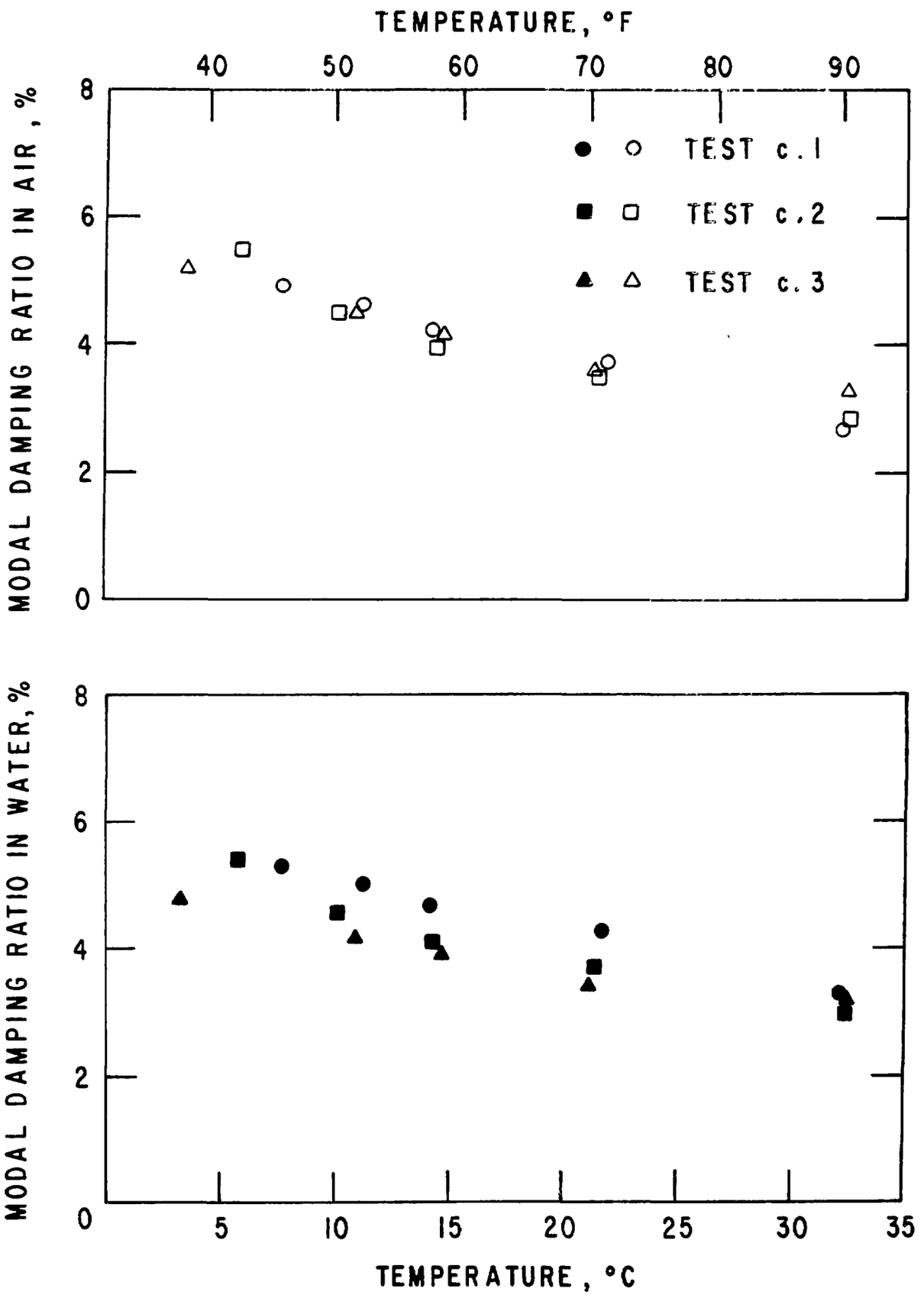

Fig. 32. Modal Damping Ratios in Air and Water for Tests c.1, c.2 and c.3

Typical tube displacements as functions of flow velocity are given in Figs. 33 and 34. Tube motion in the lift direction at instability is larger than that in the drag direction. Figure 33 shows the tube displacement components of a detuned tube array; tube 3 is unstable, while tube 4 is still stable.

Figures 35 and 36 show the typical frequency spectra of tube displacements. In Fig. 35, at low flow velocities, the dominant tube response frequency is about 35 Hz, and at high flow velocities it is shifted to about 27 Hz. In Fig. 36, at instability (3.23 m/s), all tubes oscillate at the same frequency of about 37 Hz.

Results of Tests c.1, c.2, and c.3 are given in Table 3. The basic behavior of finned tubes is similar to that of plain tubes. However, the oscillation amplitudes at instability are not as large as for plain tubes.

IV. DISCUSSIONS OF THEORETICAL AND EXPERIMENTAL RESULTS

The critical flow velocities ($U_m/f_v D$) for various tests are given in Figs. 37-39, plotted as functions of δ_m. Analytical results for Test a.1 are also given in Fig. 37.

Figure 37 shows that there are multiple stable and unstable regions. Once the flow velocity is increased to the lowest critical flow velocity, large tube oscillations will develop. However, it takes time for tubes to develop large-amplitude oscillations. If the flow velocity is increased very rapidly passing through the unstable region, large tube oscillations will not occur and the tubes remain stable. On the other hand, if the flow velocity is increased slowly so that tubes will execute large-amplitude oscillations in the unstable zone, the tubes may not regain stability because of nonlinear effects. For heavy tubes, the buildup of large oscillations is slow; for thin-wall tubes, instability will develop much more rapidly.

The upper and lower bounds of the instability regions in Fig. 37 are associated with the same mode in which the tubes oscillate predominantly in the lift direction and out of phase with respect to the neighboring tubes. Mathematically, this can be explained by the fluid-damping coefficients. In this range of reduced flow velocity, fluid-damping coefficients $\dot{\alpha}_{11}$ and $\dot{\alpha}_{12}$ are the two dominant coefficients, that cause the instability. In this range of U_r, $\dot{\alpha}_{11}$ and $\dot{\alpha}_{12}$ have opposite signs; therefore the tube motions of the two neighboring tubes must be out of phase. In the other flow-velocity range, $\dot{\alpha}_{11}$ and $\dot{\alpha}_{12}$ change sign and the tubes will not lose stability by the damping mechanism.

Test a.1 is apparently the first experiment to demonstrate the existence of multiple stable and unstable regions for tube arrays in crossflow.

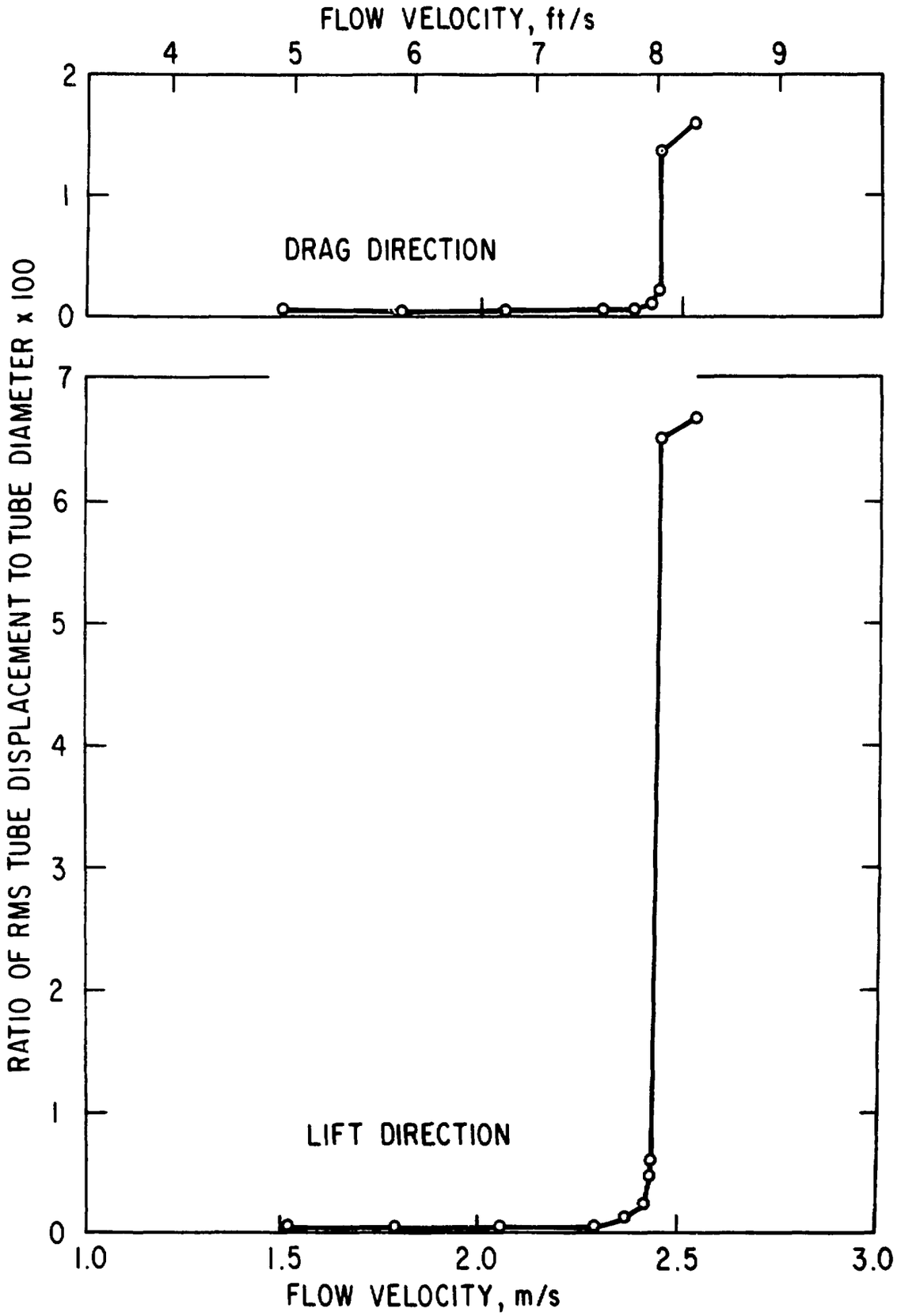

Fig. 33. Displacements of Tube 4 in Test c.1 at 14.28°C

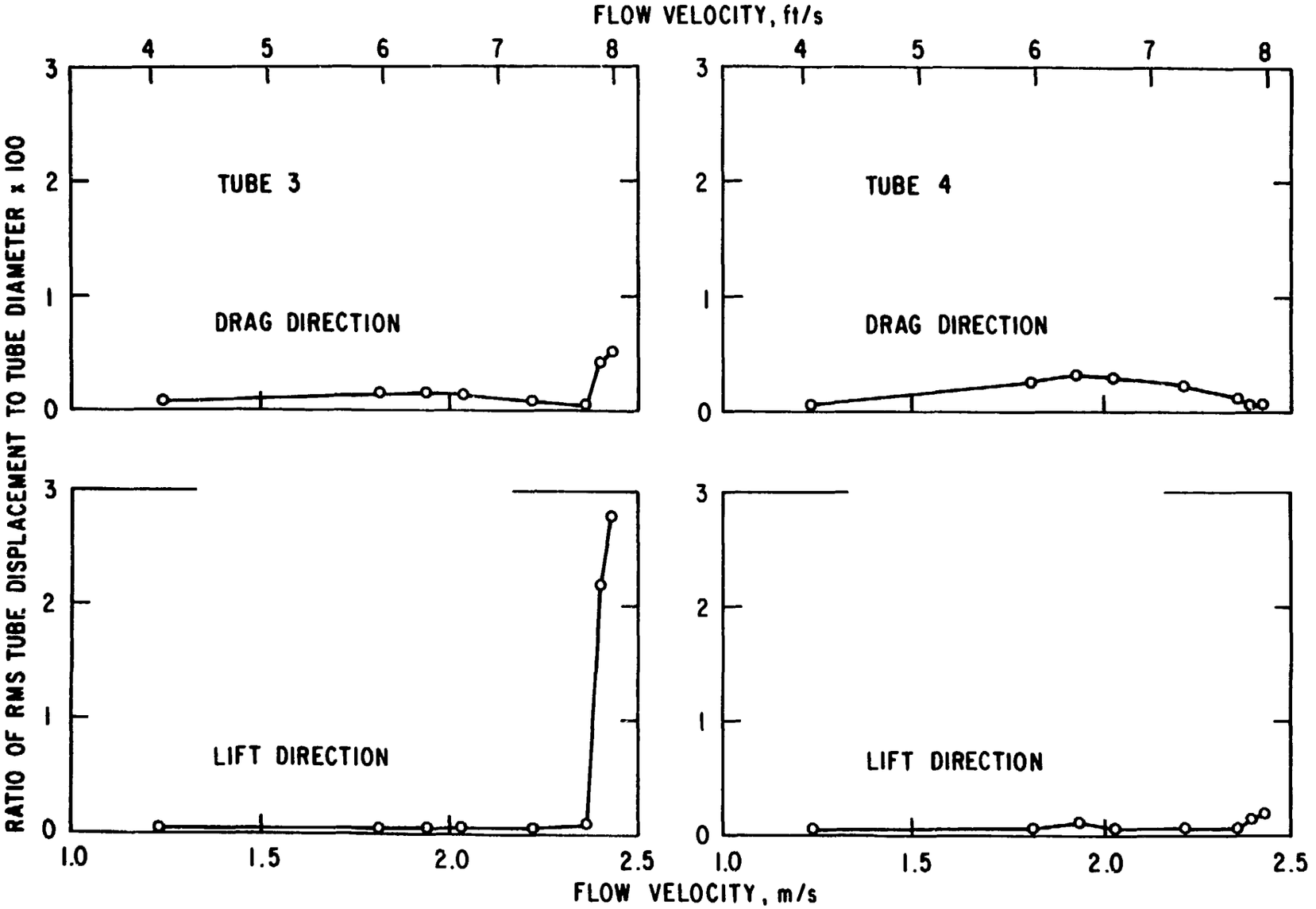

Fig. 34. Displacements of Tubes 3 and 4 in Test c.2 at 32.33°C

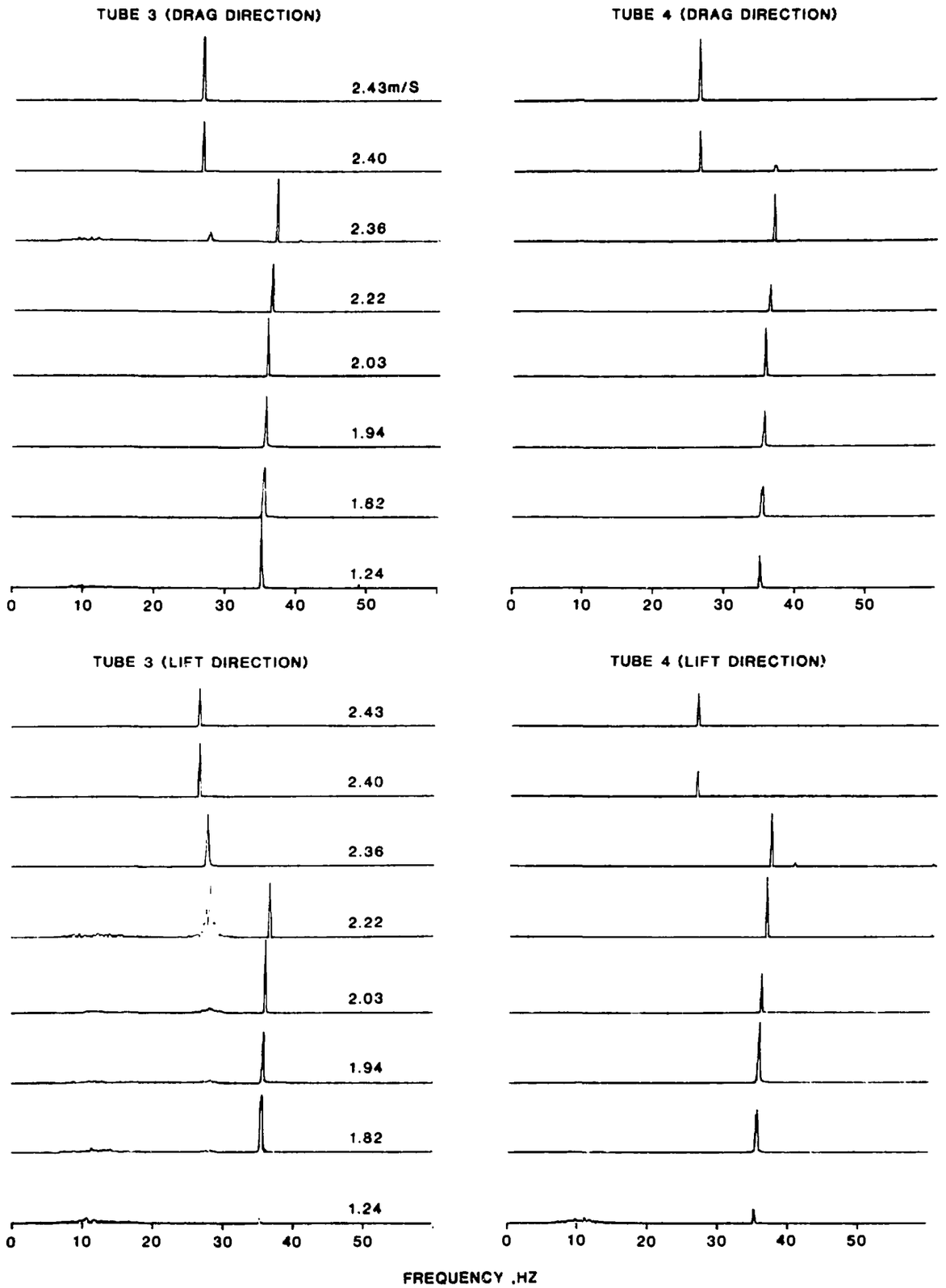

Fig. 35. Frequency Spectra of Tube Displacement for Tubes 3 and 4 in Test c.2 at 32.60°C

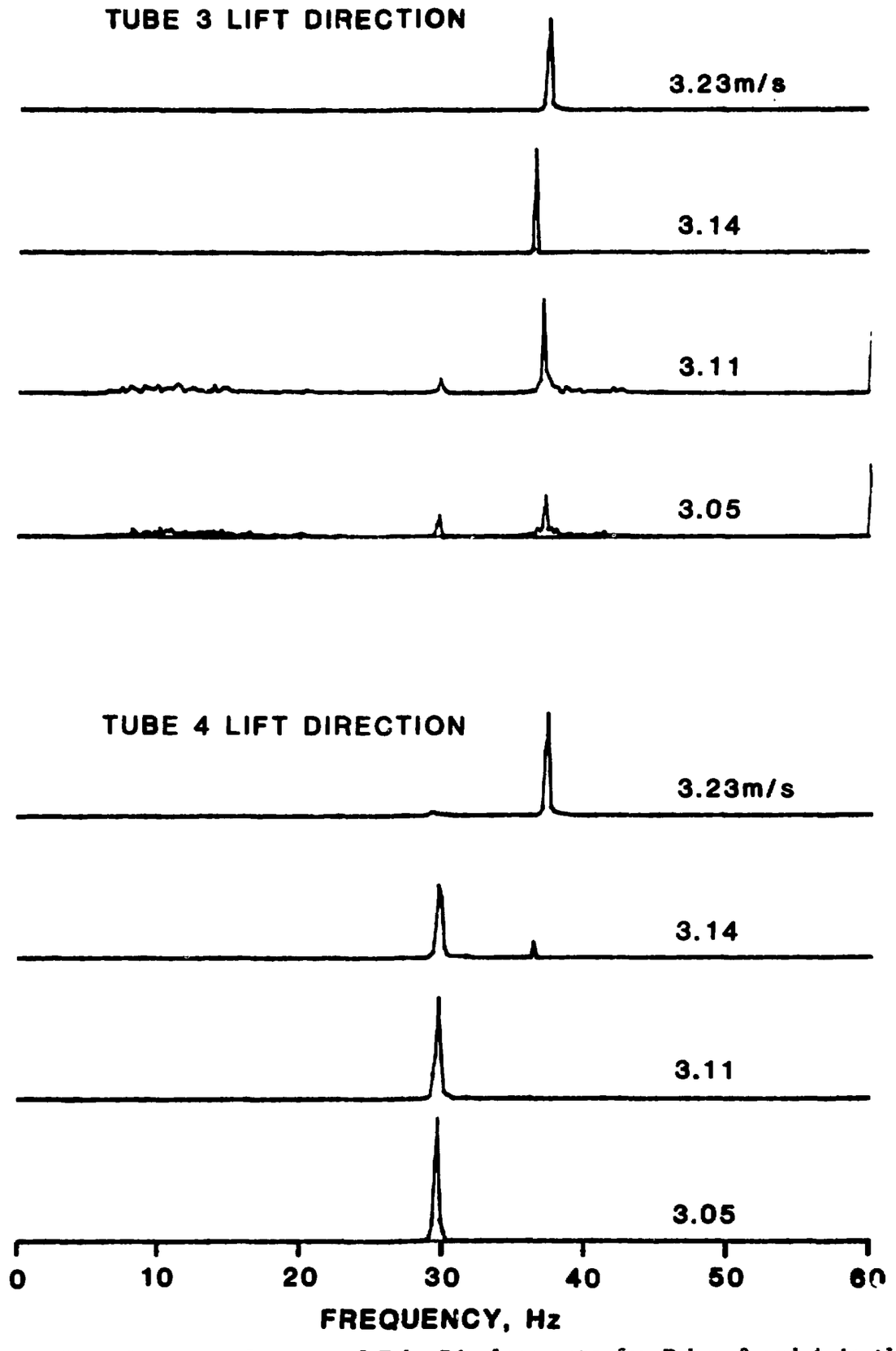

Fig. 36. Frequency Spectra of Tube Displacements for Tubes 3 and 4 in the List Direction in Test c.2 at 6°C

Table 3. Experimental Data for Tests c.1, c.2, and c.3

Test	Temperature, °C	Natural Frequency, Hz		Modal Damping Ratio, %		Oscillation Frequency at Instability, Hz	Critical Flow Velocity, m/s	$\frac{U_m}{f_v D}$	$\frac{2\pi m_v \zeta_v}{\rho D^2}$
		In Air	In Water	In Air	In Water				
	7.78	31.1	27.4	4.9	5.3	26.9	2.70	4.56	0.56
	11.22	31.0	27.3	4.6	5.0	26.2	2.55	4.31	0.52
c.1	14.28	31.3	27.5	4.2	4.7	26.6	2.45	4.11	0.47
	21.89	31.4	27.7	3.8	4.3		2.32	3.86	0.43
	32.22	31.1	27.4	2.7	3.3		2.19	3.69	0.31
	6.00	31.7	27.7	5.5	5.4	37.1[a]	3.20		
	10.11	31.4	27.5	4.5	4.6	27.6	2.96	4.94	0.51
c.2	14.44	31.2	27.3	4.0	4.0	26.8	2.65	4.46	0.45
	21.50	31.0	27.1	3.6	3.7	26.7	2.47	4.18	0.41
	32.60	30.7	26.9	2.8	3.0	26.5	2.38	4.07	0.32
	3.50	32.1	27.6	5.2	4.8	27.8	2.94	4.82	0.59
	10.94	31.6	27.2	4.5	4.2	26.7	2.51	4.18	0.51
c.3	14.67	31.3	26.9	4.2	3.9	26.6	2.50	4.21	0.47
	21.17	31.2	26.9	3.6	3.4	26.3	2.36	3.97	0.41
	32.33	31.1	26.8	3.4	3.2	26.1	2.28	3.84	0.38

[a]Instability associated with tubes 1, 2, 4, and 5.

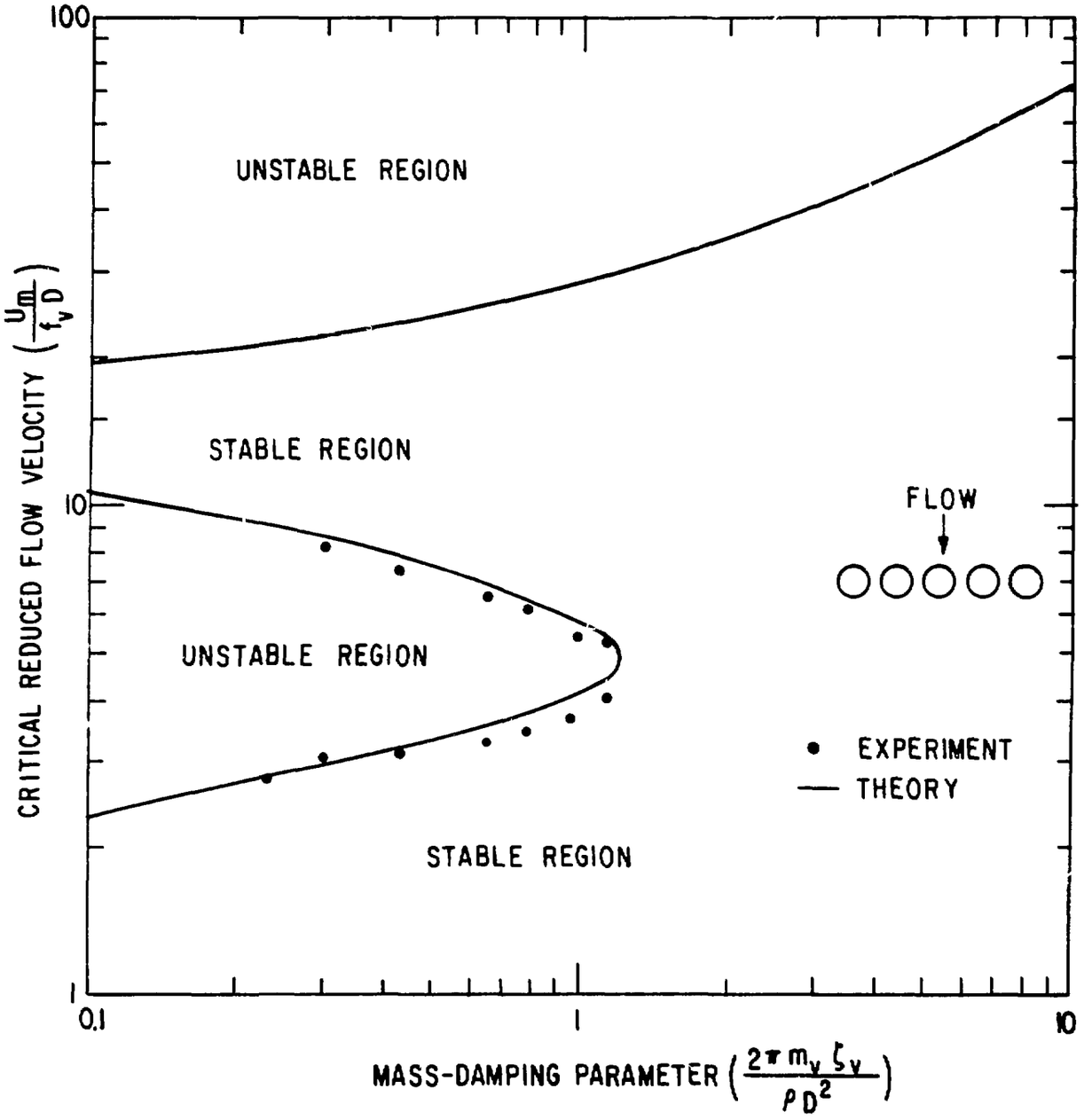

Fig. 37. Stability Map for Test a.1

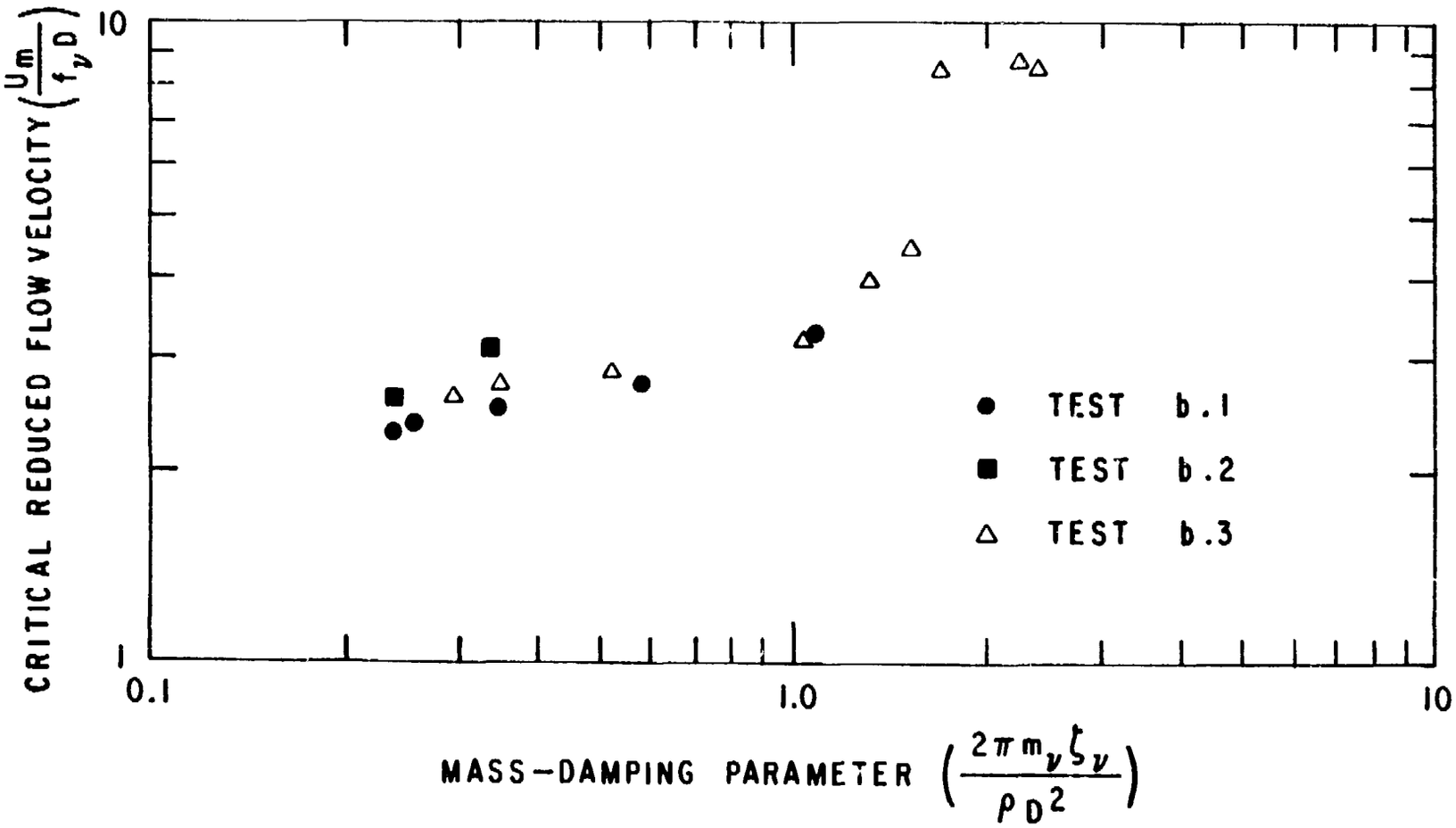

Fig. 38. Stability Map for Tests b.1, b.2, and b.3

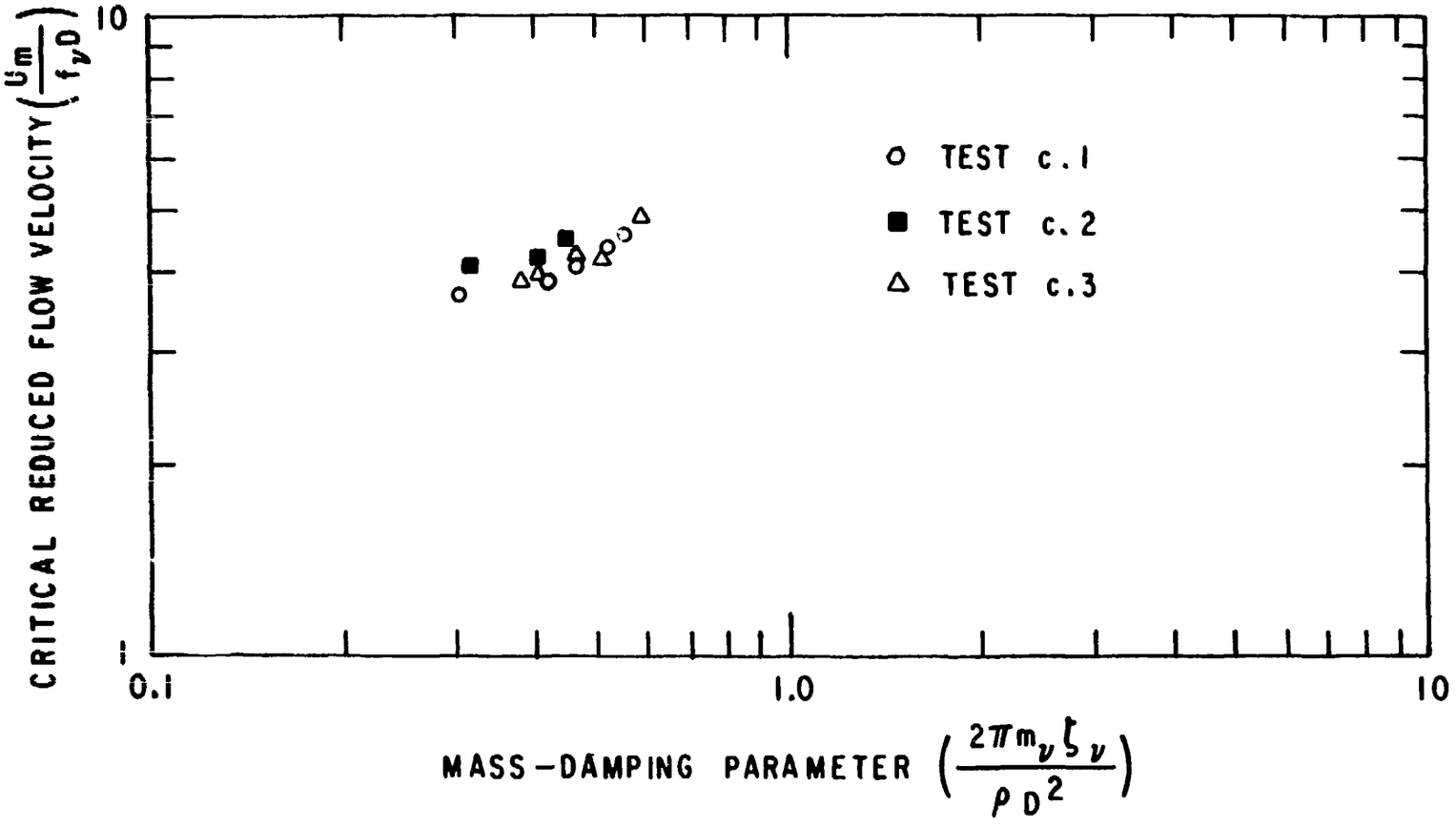

Fig. 39. Stability Map for Tests c.1, c.2, and c.3

For practical applications, the lower critical flow velocity is of importance. The higher instability boundaries are more of academic interest. For tube arrays in liquid flow (e.g., Refs. 10 and 11), there are local peaks in the response curves. Whether these peaks are associated with the multiple stable and unstable regions remains to be studied.

The lowest critical flow velocity is not necessarily associated with the lowest frequency of the tubes. Tests b.2 and c.2 have demonstrated that some of the lowest critical flow velocities are associated with the tubes with a higher frequency; this is attributed to the nonuniform flow distribution as well as fluid coupling. In practical heat-exchanger tube banks, the tube supports and flow-velocity distribution are much more complicated. The modes other than the one associated with the lowest frequency may become unstable.[8,12]

The jump of the lowest critical flow velocity at a certain value of δ_m is demonstrated in Tests a.1 and b.3. The jump is attributed to the transition from one instability mechanism to another. At low δ_m, the instability is attributed to the fluid-damping-controlled type, while at higher δ_m it is attributed to the fluidelastic-stiffness-controlled type. The values of δ_m at which the jump in the critical flow velocity obtained from analysis and experiment agree reasonably well.

Detuning in frequency, as demonstrated in Tests b.2 and c.2, tends to stabilize the tube arrays. In these tests, the instability is of fluid-damping-controlled type and the effect of detuning is not very significant. The results agree qualitatively with the analytical results given in Fig. 10.

Comparing the lowest critical flow velocities of Tests a.1 and b.1, the critical flow velocity is higher for Test a.1. This is consistent with the experimental data obtained by Ishigai et al.,[13] who show that the critical flow velocity decreases with decreasing pitch-to-diameter ratio.

The instability of finned tubes has not been reported in literature. The results of Tests b.1 and b.2 with Tests c.1 and c.2, which are plotted in Fig. 40, show that the critical flow velocity for finned tubes is higher than the corresponding plain tubes and, at instability, tube-oscillation amplitudes are smaller. Thus, based on stability consideration, finned tubes are better than plain tubes.

Figure 41 shows the lowest critical flow velocities for Test a.1 and previous test results,[3] in which the tube arrangement is identical to Test a.1, except with thin-wall tubes (wall thickness, 0.79 mm). The theoretical results and experimental data agree reasonably well. Comparison of these two tests demonstrates several features:

• The jump in the critical flow velocity (the transition of one instability mechanism to another) occurs at a δ_m that depends on the mass

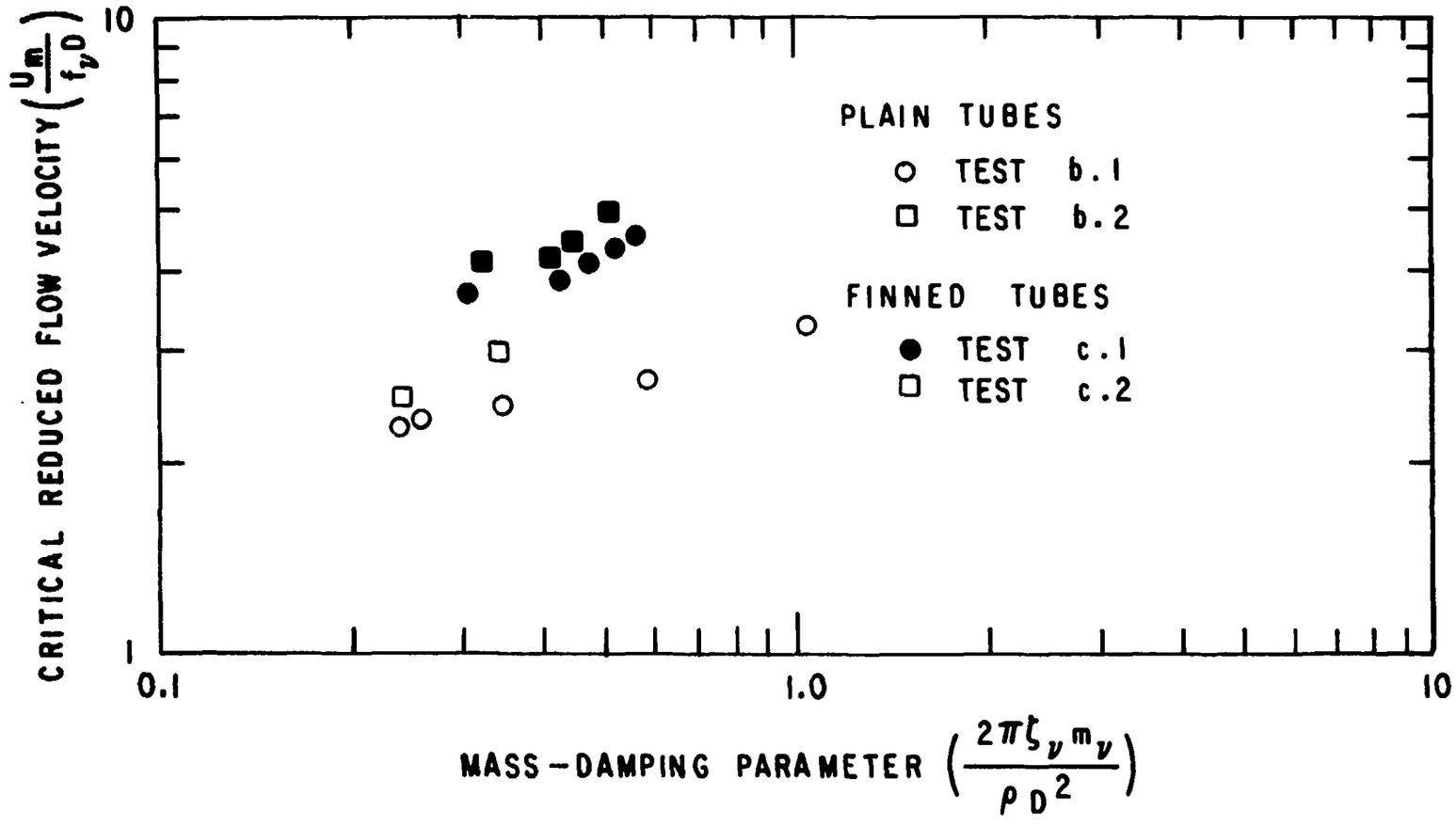

Fig. 40. Comparison of Critical Flow Velocities for Tests b.1 and b.2 with Tests c.1 and c.2

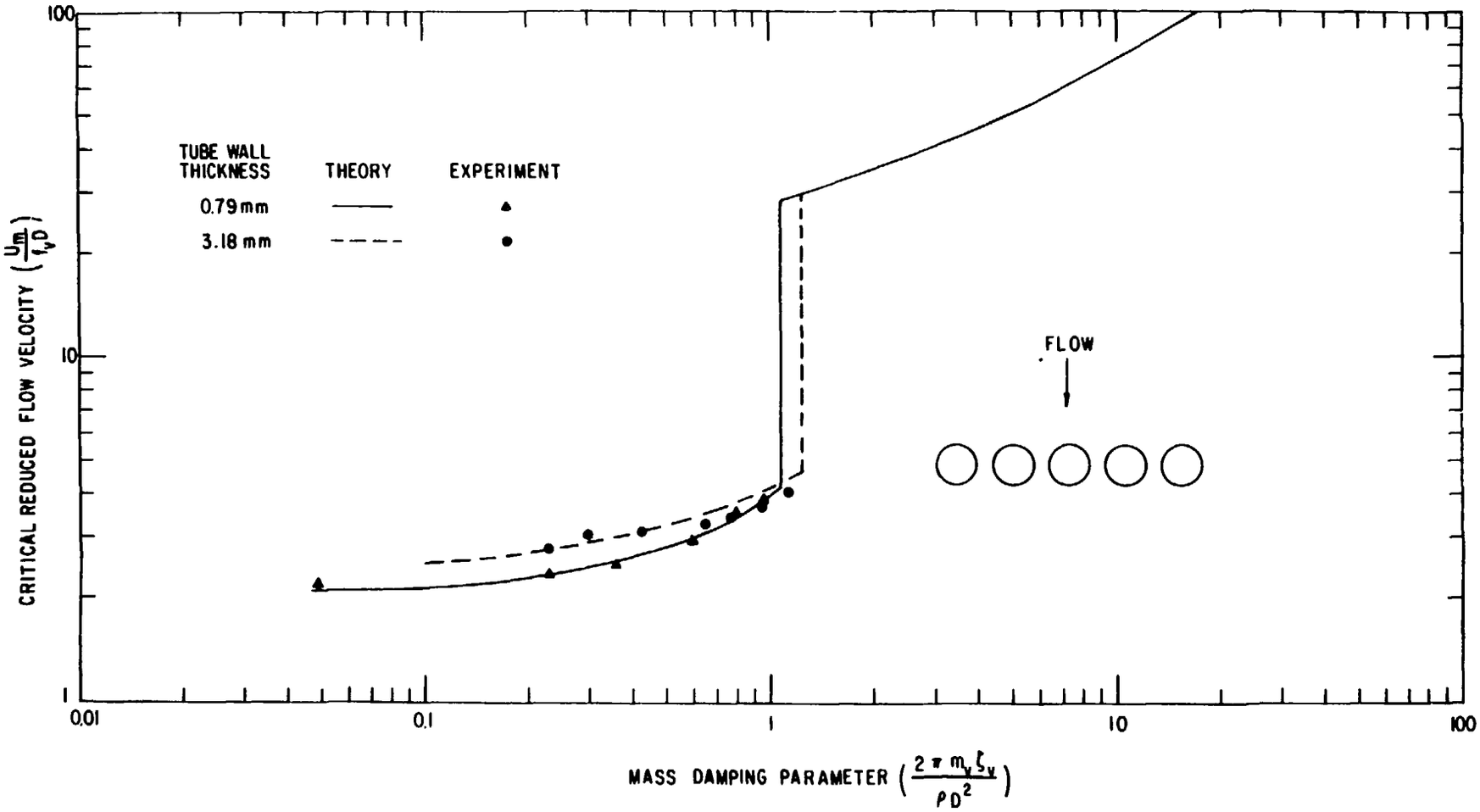

Fig. 41. Effect of Tube Mass on the Critical Flow Velocity

ratio. Both experimental and analytical results show that the transition for heavy-wall tubes occurs at larger δ_m.

• Except near the transition region, for a fixed δ_m the critical flow velocity for the thin-wall tube is lower. Both theoretical results and experimental data agree well.

• The mechanism for the two tests are basically the same, although at instability, the tube motion for thin-wall tubes is much larger.

V. CONCLUSIONS

This report presents an experimental and analytical study of tube rows subjected to crossflow. Based on the results, the following conclusions can be drawn:

• Two different distinct instability mechanisms exist for tube rows subjected to crossflow: fluid-damping-controlled instability and fluid-elastic-stiffness-controlled instability. At low δ_m, it is the fluid-damping-controlled type, and at high δ_m, it is the fluidelastic-stiffness-controlled type. There is a jump in the lowest critical flow velocity in the transition region of the two different mechanisms.

• For fluid-damping-controlled instability, the tubes oscillate predominantly in the lift direction and out of phase with respect to the adjacent tubes. For fluidelastic-stiffness-controlled instability, the tubes oscillate in a whirling pattern, with the middle tube moving predominantly in the drag direction and the two wing tubes in the lift direction, so that when the middle tube moves downstream there is a smaller gap.

• The transition from one instability mechanism to another occurs at a particular value of mass-damping parameter δ_m. The magnitude of δ_m is about an order of 1. It depends on tube spacing, mass ratio, flow-velocity distribution, and possibly other parameters.

• At high δ_m, the mass ratio and damping can be combined as a single mass-damping parameter. The critical flow velocity depends on the mass-damping parameter but varies very little with the individual values of mass ratio and damping. Therefore, the critical flow velocity can be calculated as follows:

$$\frac{U_m}{f_v D} = \alpha \left(\frac{2 m_v \zeta_v}{\rho D^2} \right)^{0.5} . \tag{38}$$

• At low δ_m, the critical flow velocity depends on the individual values of mass ratio and damping. The two parameters in general cannot be combined as a single parameter. Therefore, the critical flow velocity can

be calculated as follows:

$$\frac{U_m}{f_v D} = \beta_1 \zeta_v^{\beta_2} \left(\frac{m_v}{\rho D^2}\right)^{\beta_3}. \tag{39}$$

• There are multiple stable and unstable regions for tube rows in liquid flow. This study demonstrates, for the first time, the existence of multiple-stability regions.

• For tube rows with the same tube diameter and damping value, the tubes with thicker walls have the higher critical flow velocity and their response at instability is not as violent as for thinner tubes.

• The effect of the finned tube is to increase the critical flow velocity and to decrease the oscillation amplitude at instability. Therefore, finned tubes are beneficial in controlling tube instability.

• Detuning of tubes is beneficial in stabilizing tube rows. However, the effect of detuning depends on instability mechanisms and the amount of detuning. Furthermore, in some special situations, detuning of tubes may not always stabilize the tube arrays.

• The important parameters in determining the fluid-damping-controlled instability are $\dot{\alpha}_{ii}$, while in determining fluidelastic-stiffness instability they are $\dot{\alpha}_{ij}$ and $\dot{\tau}_{ij}$ with $i \neq j$.

ACKNOWLEDGMENTS

This work was performed under the sponsorship of the Office of Reactor Research and Technology, U. S. Department of Energy.

Acknowledgment is extended to Dr. M. W. Wambsganss for his encouragement and review of this report.

REFERENCES

1. Chen, S. S., "Design Guide for Calculating the Instability Flow Velocity of Tube Arrays in Crossflow," ANL-CT-81-40, Dec. 1981.

2. Chen, S. S., "Mathematical Model, Instability Mechanisms, and Stability Criteria of a Group of Circular Cylinders Subjected to Crossflow," ANL-CT-81-22, May 1981.

3. Chen, S. S., and Jendrzejczyk, J. A., "Experiment and Analysis of Instability of Tube Rows Subject to Liquid Crossflow," ANL-CT-81-29, Sept. 1981.

4. Tanaka, H., "A Study on Fluid Elastic Vibration of a Circular Cylinder Array (One-Row Cylinder Array)," Trans. Jpn. Soc. Mech. Eng. B 46(408), 1398-1407 (1980).

5. Tanaka, H., Takahara, S., and Ohta, K., "Flow-Induced Vibration of Tube Arrays With Various Pitch-to-Diameter Ratios," J. Pressure Vessel Technol., Trans. ASME 104, 168-174 (1982).

6. Tanaka, H., and Takahara, S., "Unsteady Fluid Dynamic Force on Tube Bundle and its Dynamic Effect on Vibration," Flow-Induced Vibration of Power Plant Components (ed., M. K. Au-Yang), ASME, New York, 1980.

7. Connors, H. J., "Fluidelastic Vibration of Heat Exchanger Tube Arrays," Trans. ASME, J. Mech. Design 100, 347-353 (1978).

8. Pettigrew, M. J., Sylvestre, Y., and Campagna, A. O., "Vibration Analysis of Heat Exchanger and Steam Generator Designs," Nucl. Eng. Des. 48, 97-115 (1978).

9. Soper, B. M., "The Effect of Tube Layout on the Fluidelastic Instability of Tube Bundles in Cross Flow," Flow-Induced Heat Exchanger Tube Vibration - 1980, ASME (eds., J. M. Chenoweth and J. R. Stenner), pp. 1-9 (1980).

10. Chen, S. S., and Jendrzejczyk, J. A., "Experiments on Fluid Elastic Instability in Tube Banks Subjected to Liquid Cross Flow," J. Sound Vib. 78(3), 355-381 (1981).

11. Weaver, D. S., and Koroyannakis, D., "The Cross-Flow Response of a Tube Array in Water - A Comparison with the Same Array in Air," J. Pressure Vessel Technol., Trans. ASME 104, 139-146 (1982).

12. Chen, Y. N., "Criteria for the Cross-flow-induced Tube Vibrations in Tube Bank Heat Exchanger," Int. Conf. Vibration in Nuclear Plant, Keswick, U.K., May, 1978.

13. Ishigai, S., Nishikawa, E., and Yagi, E., "Structure of Gas Flow and Vibration in Tube Bank with Tube Axes Normal to Flow," Int. Symp. Marine Engineering, Tokyo, pp. 1-5-23 to 1-5-33 (1973).